npj | science of food

Article

Published in partnership with Beijing Technology and Business University & International Union of Food Science and Technology

https://doi.org/10.1038/s41538-025-00479-8

Microbial succession and interaction in vacuum-packed beef: a longitudinal study of bacterial and fungal dynamics

Check for updates

Franz-Ferdinand Roch[1] ✉, Monika Dzieciol[1], Cameron R. Strachan[2], Muhammad Sharjeel Chaughtai[1], Narciso M. Quijada[3], Tea Movsesijan[2] & Evelyne Selberherr[1]

The microbial dynamics of vacuum-packed (VP) beef are shaped by interactions between bacterial and fungal communities, influencing spoilage and meat quality during storage. While bacterial succession is well studied, fungal roles remain underexplored. We examined microbial communities in VP beef over 85 days using spike-in, qPCR, 16S/18S rRNA gene amplicon sequencing, culture-based methods, whole genome sequencing, and co-culture experiments. Initially dominated by *Pseudomonas* and *Brochothrix*, the bacterial community shifted toward lactic acid bacteria (LAB) by day 15. Fungal communities remained diverse, with *Kurtzmaniella*, *Barnettozyma*, *Debaryomyces*, and *Yarrowia* as key genera. Co-culture experiments revealed a triangular interaction: yeasts enhanced LAB, LAB inhibited Enterobacterales, and Enterobacterales suppressed yeasts. Genomic analyses suggest yeast metabolites support LAB, LAB inhibit via acids and bacteriocins, and Enterobacterales produce fungal cell wall-degrading enzymes. These findings highlight fungi's overlooked role and the importance of inter-kingdom interactions in meat microbiomes, offering a foundation for strategies to improve meat safety and shelf life.

Global meat consumption has increased since 1990, rising from 153,911 tons per year to 333,883 tons in 2022[1]. The per capita consumption of beef and veal declined slightly during this period (from 6.56 kg capita^{-1} year^{-1} to 6.28 kg capita^{-1} year^{-1}), but due to global population growth, total consumption increased from 48,002 tons to 75,728 tons[1]. Meat is considered an important source of essential nutrients and protein, playing a significant role in the human diet. However, the rise in global meat consumption has led to major environmental challenges. Meat production requires substantial amounts of resources, including land, water, and feed, and contributes to deforestation, greenhouse gas emissions, water pollution, and biodiversity loss[2]. The environmental impacts of meat production, as well as food production in general, are addressed in the United Nations Sustainable Development Goals (SDGs). One of these SDGs (SDG 12) focuses on sustainable consumption and production patterns, including the reduction of food waste, as approximately one-third of all food produced globally is wasted[3]. Additional goals, such as SDG 2 (zero hunger) and SDG 13 (climate action), also highlight the importance of sustainable and efficient food systems. In meat production, inefficient management, such as improper handling and storage during production and distribution, can lead to spoilage, foodborne illnesses, and ultimately food waste and public health risks. Addressing these challenges requires a comprehensive understanding of microbial dynamics involved in meat preservation and the impact on food safety and shelf life.

Vacuum-packaging is widely used in the meat industry to extend shelf life, preserve meat quality, and reduce spoilage by limiting oxygen availability, thereby slowing oxidative degradation and inhibiting the growth of aerobic spoilage microorganisms. However, the absence of oxygen can favor the proliferation of facultative and obligate anaerobes, including lactic acid bacteria (LAB), which can contribute to both preservation and spoilage, depending on species composition and storage conditions, and Enterobacterales, potentially impacting the quality and safety of the meat[4,5]. The microbial dynamics in vacuum-packed beef are complex and influenced by a variety of factors, including temperature, pH, water activity, and interactions with other microorganisms, such as competition, mutualism, and antagonism[6]. While LAB are often associated with protective effects (e.g., acidification, competitive exclusion, and bacteriocin production), they can also contribute to spoilage by producing off-odor compounds[7]. The same genera (e.g., *Latilactobacillus*, *Leuconostoc*, *Lactococcus*) can exhibit both beneficial and spoilage activities depending on environmental conditions and interactions with other community members[7]. Spoilage of fresh

[1]Clinical Department for Farm Animals and Food System Science, Center for Food Science and Veterinary Public Health, University of Veterinary Medicine Vienna, Veterinärplatz 1, 1210 Vienna, Austria. [2]Austrian Competence Centre for Feed and Food Quality, Safety and Innovation, FFoQSI GmbH, Tulln an der Donau, Austria. [3]Institute of Functional Biology and Genomics (IBFG), CSIC - University of Salamanca, Salamanca, Spain. ✉e-mail: franz-ferdinand.roch@vetmeduni.ac.at

vacuum-packed beef has been associated with a wide range of bacterial genera, including *Acinetobacter*, *Pseudomonas*, *Brochothrix*, *Psychrobacter*, *Moraxella*, lactic acid bacteria (LAB), and Enterobacterales[8–11]. In addition to slime-formation, gas production, drip loss, and discoloration, off-odors are of particular importance[12]. Spoilage usually occurs when specific spoilage organisms reach unacceptable levels, causing their metabolites, such as alcohols, aldehydes, ketones, esters, volatile fatty acids, and sulfur compounds, to accumulate in the meat[13]. A series of studies conducted in recent years has examined the succession of these spoilers and their contribution to meat deterioration or the shift in community composition in longitudinal studies. *Psychrobacter*, *Acinetobacter*, *Pseudomonas*, and *Moraxella* are mainly dominant in the early phases of storage[14,15], and are then replaced by lactic acid bacteria as the dominant taxa within a few days, depending on the storage temperature[16,17]. *Clostridia* are typically found in higher quantities in later phases[18].

Research on ripening and spoilage on vacuum-packed meat has primarily focused on bacteria, while the role of fungi remains understudied and often underestimated[19,20]. Fungi, which are integral to many food ecosystems, may also play a pivotal role in the microbial dynamics of vacuum-packed beef, both through direct spoilage mechanisms and indirect modulation of bacterial communities. Fungi are known to produce a wide range of secondary metabolites, including organic acids, alcohols, and volatile compounds, which can significantly alter the physicochemical environment[20]. For instance, Kabisch et al. showed the direct contribution of *Kazachastania* to gas production, accelerating spoilage[21], while Hultman et al. detected yeast RNA in late-stage spoilage samples, suggesting active fungal involvement in spoilage processes[19]. The impact of fungi on the bacterial community has been shown in other food ecosystems. For example, *Debaryomyces hansenii*, *Geotrichum candidum*, and *Penicillium camemberti* deacidify the surface of cheese, which can lead to the growth of less acid-tolerant bacteria[22]. Similarly, *Galactomyces geotrichum*, *Debaryomyces hansenii*, and *Penicillium* sp. can shift the microbial community composition[23]. The enzymatic activity of fungi, including the activity of proteases and lipases, may also contribute to the breakdown of complex proteins and fats in meat, creating substrates that can be utilized by bacteria, thereby indirectly accelerating spoilage. Fungal-bacterial interactions may also involve competition for nutrients, with fungi potentially outcompeting bacteria for key substrates, thereby delaying bacterial growth and altering the spoilage trajectory.

In this study, we investigated the microbial dynamics on vacuum-packed beef using different cultivation-free and cultivation-based techniques. By integrating the analysis of both bacterial and fungal components in vacuum-packed beef, our research aims to bridge this knowledge gap and shed light on the often overlooked but potentially crucial role of fungi in meat spoilage and the complex cross-kingdom interactions that might occur during ripening and subsequent spoilage. Preliminary observations revealed frequent co-occurrence of species from different kingdoms, suggesting that cross-kingdom interactions play a key role in shaping microbial community dynamics and functional outcomes over time, beyond the effects of individual taxa. Further, we propose that yeast-derived metabolites might have the ability to enhance the growth of LAB on vacuum-packed beef, thereby influencing microbial succession. Expanding on this, we hypothesize that yeasts, LAB, and Enterobacterales form a "triangle of interactions", collectively driving microbial dynamics and functionality within the ecosystem.

Results

Distinct growth dynamics observed for bacteria and fungi

To explore the microbial succession and potential spoilage dynamics during storage, we monitored bacterial and fungal growth on vacuum-packed striploins over 85 days. Viable cell counts were determined using multiple culture media to quantify mesophilic bacteria and fungi and to identify potential candidates for downstream co-culturing experiments. The culture growth experiments showed that the mesophilic bacteria grew from 3.97 $\log_{10}$ CFU g^{-1} (SD ± 0.45) on day 0 to a plateau of 7.5 $\log_{10}$ CFU g^{-1} (SD ± 0.35) between day 15 and 20 (Supplementary Fig. 1). The LAB arose from 3.05 $\log_{10}$ CFU g^{-1} (SD ± 0.46) on day 0 to 7.46 $\log_{10}$ CFU g^{-1} (± 0.38) on day 15. The Enterobacterales, exhibited substantial individual variations among the different cuts of meat, ranging from 1.24 $\log_{10}$ CFU g^{-1} (SD ± 1.43) on day 0 to 5.85 $\log_{10}$ CFU g^{-1} (SD ± 0.69) on day 15. The colony-forming units on fungal culture plates (BR and YGC with 4 °C and 25 °C incubation) raised from 1.82 (SD ± 1.08), 2.3 (SD ± 0.96), and 2.54 (SD ± 0.42) $\log_{10}$ CFU g^{-1} on day 0 to 4.03 (SD ± 0.22), 4.37 (SD ± 0.23), and 4.14 (SD ± 0.16) $\log_{10}$ CFU g^{-1} on day 15, respectively. Some *Pseudomonas* spp. and *Serratia* spp. were able to grow on the chloramphenicol-containing fungal plates and were consistently recovered. Their presence may have influenced the fungal plate counts and should be considered when interpreting the results.

In addition to cultivation, molecular biological methods, i.e., the use of spike-in cells in amplicon sequencing and qPCR, were used to quantify the microbial community. A strong correlation was observed between plate count data and the calculated growth curves (based on the spike-in cells for bacterial data). The calculated growth curves showed consistently higher values than plate counts, which likely reflects methodological differences such as the ability of PCR to detect DNA from both live and dead cells, as well as the uncultivability of some bacteria. However, the curves themselves exhibit parallel trends (Supplementary Fig. 2), and the results are highly correlated (Pearson's $r = 0.94$, Supplementary Fig. 3a, b). On the other hand, the calculated fungal counts, based on qPCR, showed a weak correlation across all samples ($r = 0.43$). While samples from batches 1 and 2 showed strong correlations ($r = 0.76$), adding batch 3 into consideration reduced the correlation (Supplementary Figs. 2, 3c, d). In batch 3, *Serratia* levels were significantly higher compared to batches 1 and 2 (Supplementary Fig. 4). This may explain the weak correlation, as *Serratia* also grew on the fungal plates. Removing samples with a high abundance of *Serratia* ($> 10^6$) resulted in a higher Pearson correlation coefficient (0.67) between the qPCR and plate counts, compared to the full dataset (0.43, Supplementary Fig. 3c and e).

The use of spike-in cells and qPCR calculations further allowed us to estimate growth curves for the individual ASVs, species, and genera, particularly for higher-abundance taxa (Supplementary Fig. 5). In this context, we used the individual sequencing depths and the total 16S rRNA gene copies per gram of meat expected per sample to calculate the minimum population size required to be detected at least once (Supplementary Fig. 5). This clearly indicates that populations located within this detection range have a low likelihood of being detected at all. This makes it difficult to make statements about the general members of communities and, above all, to analyze interactions, as many methods assume linear relationships that are no longer given when limited by detection sensitivity. The estimation of the growth curves additionally allowed us to describe the succession of the different taxa. Despite *Pseudomonas* and *Brochothrix* reaching their growth plateau earlier than LAB (day 6 vs day 15), they were outcompeted by LAB at later timepoints. The LAB *Carnobacterium*, *Dellaglioa*, *Leuconostoc*, and *Lactococcus* reached their plateau by day 15, while *Latilactobacillus* (~ day 41) and *Enterococcus* (~ day 85) required more time (Supplementary Fig. 6). Similarly, most of the Enterobacterales (i.e., *Hafnia*, *Serratia*, *Rouxiella*, and unclassified *Enterobacteriaceae*) reached their plateau at day 15. In contrast, *Yersinia* and *Morganella* exhibited a delayed growth trajectory, requiring over 70 days to reach their respective plateaus. The succession patterns and the ratio of the target strain population size to total population size naturally also influence the likelihood of successfully isolating certain strains. Consequently, the succession patterns identified using the amplicon sequencing results align with the range of time points, when genera could be isolated from the meat samples (Supplementary Fig. 7).

In contrast to the bacterial growth curves, the fungal growth curves were less uniform. In four samples, the fungal communities exhibited peaks between days 28 and 55, typically followed by a population decline. This phenomenon is evident in both the qPCR and plate counting data (Supplementary Fig. 2). Fungal communities in batch 3, were less stable and had smaller populations compared to batches 1 and 2. The main characteristic of this unstable population is the low and unstable population of *Kurtzmaniella*, which dominated the other samples (Supplementary Fig. 8). Nine

samples (median read counts = 29), without any *Kurtzmaniella* reads were not used for downstream analysis and are consequently missing in Supplementary Fig. 8. Common genera, such as *Kurtzmaniella*, *Barnettozyma*, *Yarrowia*, and *Debaryomyces*, displayed population peaks between days 20 and 40, followed by a decline in population. *Malassezia* also showed a slow but steady population decline over the whole period of 85 days (Supplementary Figs. 9 and 10). Notably, batch 3 had a high population of *Serratia* and other "unclassified *Enterobacteriaceae*", which were isolated from fungal plates, potentially influencing fungal communities, particularly *Kurtzmaniella*.

Lactic acid bacteria dominated vacuum-packed beef by day 15 following a rapid succession of different bacteria and fungi

In total, 90 and 81 samples were subjected to 16S or 18S rRNA gene amplicon high-throughput sequencing (HTS), yielding a median of 16,895 or 280 quality control (QC) sequences per sample, respectively. *Psychrobacter*, *Brevibacterium*, and *Pseudomonas* dominated at day 0, while LAB, which would later become dominant, were still present at low abundance. A rapid and dynamic shift ensued thereafter. During the first three days *Brochothrix* and *Aeromonas* rose and dominated but were subsequently replaced by LAB, including *Carnobacterium*, *Enterococcus*, *Dellaglioa*, *Latilactobacillus*, *Leuconostoc*, and *Lactococcus*, from day 15 onwards (Fig. 1a). The succession of these bacteria correlated with a decrease in alpha diversity, as only a few species dominated (Fig. 1d, Supplementary Fig. 11). Alpha diversity was calculated using coverage-based rarefaction (iNEXT, coverage = 0.995), ensuring comparability across samples. We used Hill-Shannon ($q = 1$) and Hill-Simpson ($q = 2$) diversity indices, which account for differences in sequencing depth while maintaining robust diversity estimates. Beta diversity was assessed using Principal Coordinate Analysis (PCoA) based on Bray-Curtis dissimilarities, calculated across all samples. The PCoA plot (Fig. 1b) effectively captured the differences between bacterial communities, with clustering evident in batch 3. Overlaying the PCoA plot with taxa-based vectors highlighted taxa significantly associated with the community structure, including higher populations of *Serratia* in batch 3 and *Kurtzmaniella* in the other batches. Apart from the dominating LAB, only a few genera, including *Serratia*, unclassified *Enterobacteriaceae* (i.e., *Kluyvera*, *Buttiauxella*, based on the matching isolates), and *Clostridium*, were present in abundances over 1% relative abundance overall from day 15 onwards. As previously described for the fungal population, the microbial dynamics in batch 3 differed from those in other batches, showing higher amounts of *Serratia*, *Kluyvera*, and *Buttiauxella*. Additionally, LAB representation showed lower amounts, and the population of *Kurtzmaniella* was also reduced (Supplementary Figs. 4, 8). Accordingly, this results in a diverging cluster of batch 3 in the PCoA plot analysis, as shown in Fig. 1b. Overlaying the PCoA plot with taxa-based vectors highlights higher populations of *Serratia* in batch 3 and *Kurtzmaniella* in the other batches, along with other taxa that were consistently present across samples. Throughout the examination period, the fungal community was dominated by *Kurtzmaniella*. Other genera, consistently present, were *Barnettozyma*, *Debaryomyces*, and *Yarrowia* (Fig. 1c). While the sequencing depth for fungal communities was lower than for bacteria (median ~280 reads/sample), alpha diversity was estimated using coverage-based rarefaction (iNEXT, coverage = 0.995) to ensure comparability across samples. Under this standardization, diversity metrics remained stable across time points (Fig. 1e, Supplementary Fig. 12), although we note that absolute diversity values may be conservative due to lower sampling depth.

Since many community analysis methods assume linear relationships, while microbial interactions can be nonlinear, we applied CoNet[24] to identify associations between bacterial and fungal species. CoNet integrates both Spearman correlation and mutual information, allowing for the detection of both linear and nonlinear dependencies. This approach is particularly useful in overcoming challenges posed by detection limits, as described previously. The results showed significant connections between bacteria and fungi (Fig. 2a). Based on mutual information *Kurtzmaniella* and *Barnettozyma* exhibited direct associations with several highly abundant LAB. Bacteria that were closely associated with yeast include *Serratia* and *Brochothrix*. Other bacteria, such as *Serratia*, *Butauxiella*, *Pseudomonas*, *Psychrobacter*, and *Brevibacterium*, were indirectly associated with the fungi through interactions with other bacteria.

Taxonomic classification of cultured isolates

Overall, a total of 576 bacterial and 269 fungal isolates were collected and taxonomically classified using Sanger sequencing. Of these, 528 bacterial isolates were assigned to 41 genera, with no inconsistencies between databases (Supplementary Table 1, Supplementary Fig. 7a). The other isolates had inconsistencies between databases, hits in only one database, or were classified with a minimum bootstrap confidence interval (CI) of 90 and were summarized in Supplementary Tables 2 and 3. Among the fungal isolates, 199 isolates were assigned to 11 genera with a minimum bootstrap CI of 100. Classifications to higher taxonomic ranks or those with a bootstrap CI of 90 are listed in Supplementary Fig. 7b and Supplementary Table 4. Several genera, including *Latilactobacillus*, *Carnobacterium*, *Leuconostoc*, *Lactococcus*, *Pseudomonas*, *Serratia*, and *Kurtzmaniella*, were isolated from all three batches and persisted at least until day 56. Other genera, primarily from the classes Actinobacteria, Deinococci, and Bacteroidia, were isolated only from individual samples or during the early stages of ripening.

Based on the amplicon sequencing results and network analysis, thirteen bacterial and five yeast isolates were selected for whole-genome sequencing (WGS) and downstream co-cultivation experiments (Tables 1 and 2). The selection was primarily guided by the relative abundance of taxa in the amplicon data and their association patterns in the microbial interaction network. To focus on potentially relevant interactions, we prioritized bacterial isolates that were directly or secondarily associated with yeasts in the network. Isolates that failed to grow under the experimental conditions were excluded. For the yeast isolates, we applied less stringent filtering, retaining the most abundant taxa even if no direct bacterial association was inferred in the network, considering the limited resolution of amplicon data and the exploratory nature of the study. One of the five sequenced yeast isolates was excluded from the co-cultivation assays due to its biofilm-forming phenotype, which interfered with the experimental setup. From the original pool of 13 bacterial isolates, 10 (seven LAB and three Enterobacterales) were selected for co-cultivation with the remaining four yeast isolates, based on growth compatibility and network relevance. The batch or time point of isolation, as well as specific genomic features, were not used as selection criteria for isolates. The taxonomic assignments and genome information of the bacteria and yeast are shown in Tables 1, 2, and Supplementary Tables 5–10, respectively. All but one bacterial isolate showed an ANI of over 97% with their closest genome reference (Table 1); thus, they were given the corresponding taxonomic name. One *Lactococcus* isolate showed a low identity to its closest reference *Lactococcus raffinolactis* (GCF_001591765.1; 89.8% ANI), and was named *Lactococcus* sp. ID-0049 to avoid taxonomic misinterpretations. Two yeast isolates were classified as *Debaryomyces hansenii*, one as [*Candida*] *zeylanoides*, currently grouped in the genus *Kurtzmaniella* within the family *Debaryomycetaceae*, and the other as [*Candida*] *norvegica*, currently grouped in the genus *Barnettozyma* within the family *Phaffomycetaceae*.

Co-cultivation reveals that yeasts promote lactic acid bacteria growth

Seven LAB and three Enterobacterales strains were each co-cultured twice with four yeasts in duplicates (Supplementary Figs. 13–19) using 96-well microplates. Six out of seven co-cultures of LAB with [*C.*] *zeylanoides* and five out of seven with *D. hansenii* (ID-0991) and [*C.*] *norvegica* exhibited initially increased growth rates (Supplementary Fig. 20a). In contrast, co-cultures with *D. hansenii* ID-0368 did not show any positive effects on growth rates. For carrying capacities, *C. divergens* ID-0052 and *L. gasicomitatum* ID-1609 benefited from all four yeasts (Supplementary Fig. 20b). None of the yeasts had higher CFUs in co-culture compared to monoculture (Fig. 2b). The qPCR results showed

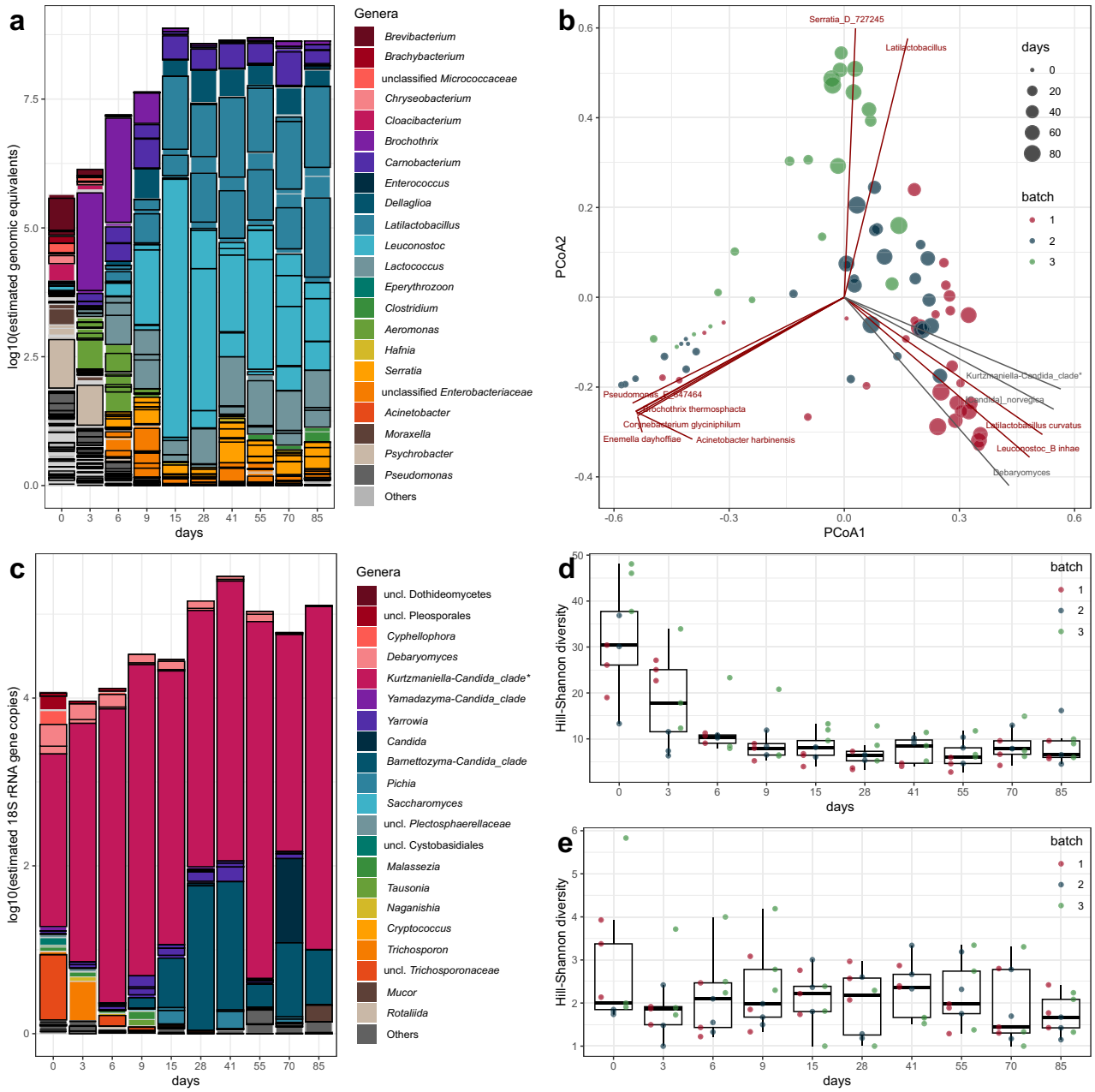

Fig. 1 | Composition and changes of the bacterial and fungal community during 85 days in vacuum-packed beef. a Mean bacteria taxa barplots for each sampling timepoint. Bar height represents the total absolute $\log_{10}$ estimated genomic equivalents, based on *Imtechella* spike-in cells. In both **a** and **c** the colored bars show the proportions of individual genera on the absolute abundance. Only genera with at least 5% relative abundance in at least one of the samples were displayed. If higher taxonomic ranks reached 5% they are displayed instead, otherwise they are shown as others. Black frame bars represent ASVs that have 100% matching sequences with isolates. Overall, 81% (16S) and 99% (18S) of the cumulated ASV counts were assigned to isolated genera with a 100% sequence match. **b** Principal Coordinate Analysis (PCoA) plot based on Bray-Curtis dissimilarities of the raw reads from 16 S and 18 S rRNA gene amplicon sequencing data. The data points represent bacterial community compositions derived from 16 S rRNA gene sequencing, with colors indicating batch effects and point sizes reflecting sampling time (days). The overlaid vectors highlight species-level associations with the principal coordinate axes. Vectors in dark red correspond to bacterial taxa from the 16 S dataset, while gray vectors represent fungal taxa identified through 18 S sequencing. Only species with significant associations ($p < 0.05$) and correlation values exceeding 0.3 (for bacteria) or 0.1 (for fungi) are displayed. **c** Mean fungi taxa barplots for each sampling timepoint. Bar height represents the total absolute $\log_{10}$ estimated 18S rRNA gene copy numbers, based on 18 S qPCR. * Taxonomy adapted, based on matching isolates. **d** Bacterial alpha-diversity (Hill-Simpson) and **e** fungal alpha-diversity (Hill-Simpson) of the samples over 85 days. Box plots show the median with hinges that correspond to the 25th and 75th percentiles. The whiskers extend from the hinge to the largest and smallest value no further than 1.5 multiplied by the inter-quartile range. The individual samples were displayed as dots, colored by batch.

different outcomes for some strains compared to the CFU counts. In particular, the strain ID-1626 (*L. carnosus*) had a significantly higher carrying capacity in co-culture with each of the yeast strains compared to monoculture when tested with qPCR, but not with CFU counts (Fig. 2b). In general, based on testing with qPCR, almost all LAB had a higher carrying capacity in co-culture with the yeasts compared to monoculture (Supplementary Fig. 20c). For the tested Enterobacterales, none of the co-cultures demonstrated clear positive effects on the growth rates. The evaluation of the carrying capacity is not clearly reproducible, which suggests that the effect of the yeasts on Enterobacterales is small. On the

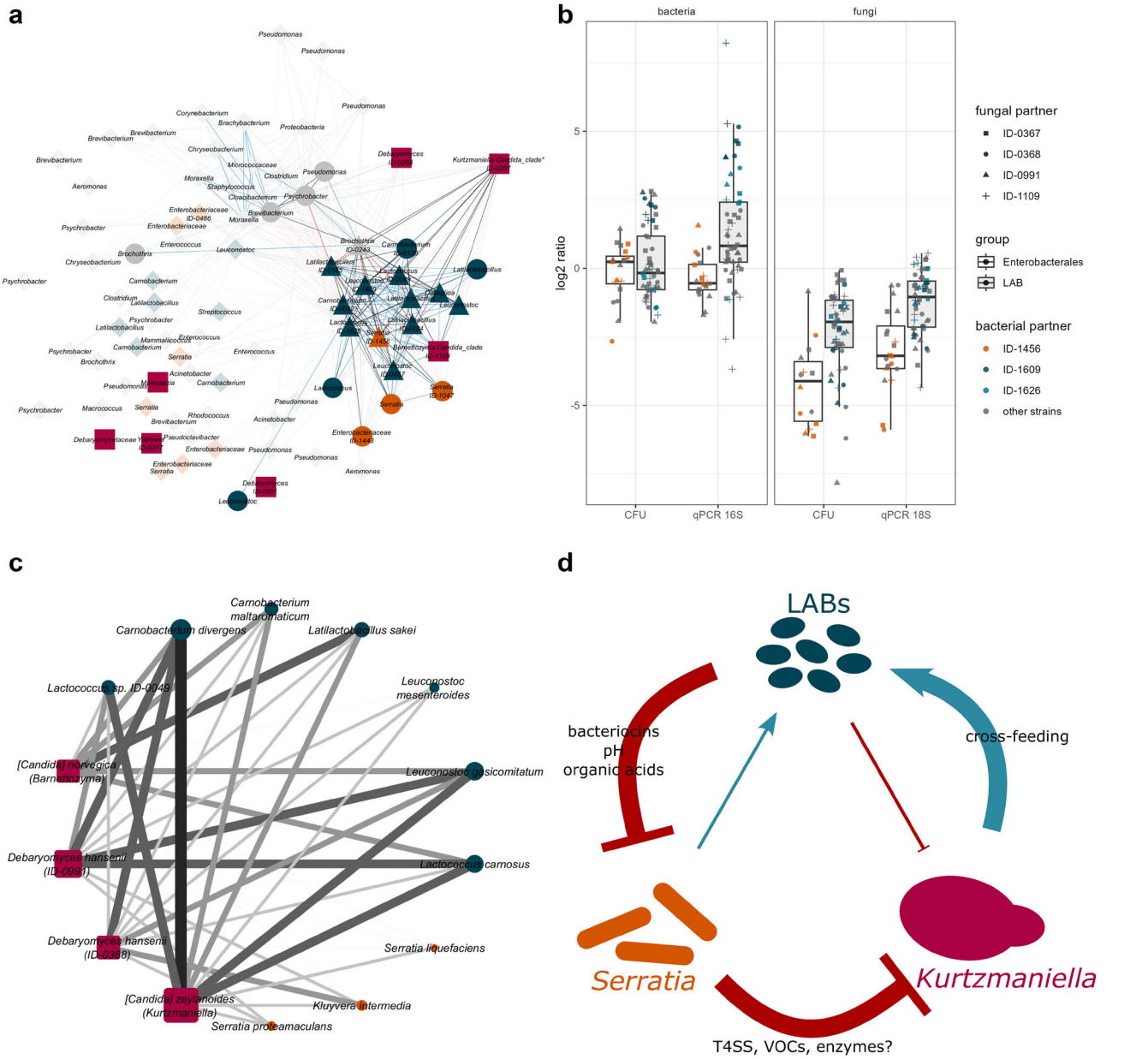

Fig. 2 | Bacterial fungal interactions. a CoNet network analysis of bacterial-fungal interactions, displaying significant co-occurrence patterns. Black edges represent associations based on mutual information, while red and blue edges indicate negative and positive correlations, respectively (Spearman correlation). Node colors distinguish microbial groups: lactic acid bacteria (LAB) in blue, *Serratia* and unclassified Enterobacterales (including *Kluyvera* and *Butauxiella*) in orange, and other bacteria in grey. Fungi are shown as pink squares. Node shapes indicate interaction levels: circles represent bacteria directly associated with yeasts, triangles indicate second-order bacterial associations, and diamonds represent other bacterial taxa. * Taxonomy adapted, based on matching isolates. **b** Growth interactions in bacterial--yeast co-cultures measured by colony-forming units (CFU) and qPCR. The plot shows the $\log_2$ ratio of microbial abundance in co-cultures relative to monocultures. A $\log_2$ ratio > 0 indicates a higher final abundance in co-culture (suggesting a positive effect), while values < 0 indicate growth inhibition. The left panel shows bacterial data, the right fungal data, each split by method: CFU enumeration or qPCR-based 16S/18S rRNA gene quantification. Boxplots summarize the distribution of $\log_2$ ratios across strain combinations. Points represent individual co-culture experiments. Bacterial partners belong to either Enterobacterales (white boxes) or LAB (grey boxes). Box plots show the median with hinges that correspond to the 25th and 75th percentiles. The whiskers extend from the hinge to the largest and smallest value no further than 1.5 multiplied by the inter-quartile range. Point shapes indicate the fungal strain used in each co-culture. **c** Summary of the co-culture and supernatant experiments showing the positive effects of yeasts on the tested bacteria. The color intensity and line width represent the cumulative number of positive effects, including increased initial growth rate, elevated carrying capacities (qPCR, CFU) in co-cultures, and enhanced OD in supernatant experiments. **d** Simplified schematic representation of the triangular relationship between *Kurtzmaniella*, *Serratia*, and LAB.

other hand, the Enterobacterales had an adverse effect on the growth of the yeasts. This was especially pronounced for *S. proteamaculans* ID-1456 (Fig. 2b). Overall, the co-culture experiments suggested a positive effect of yeasts on the growth of LAB, but not on the growth of Enterobacterales, while the yeasts are negatively affected by both groups, but much more by the Enterobacterales.

Yeast cell-free supernatants enhance the growth of lactic acid bacteria, but the effect is strain specific

Cell-free supernatants from four yeast strains were tested for their effects on the growth of LAB (Supplementary Figs. 21–26). The supernatants were collected after 48 h of incubation and added to the LAB cultures at two dilution ratios (1:2 and 1:4 in fresh medium). The growth of the LAB was

Table 1 | Bacterial isolates and their GTDB-based closest classification, placement reference, and genome ANI

Internal ID	Closest genome taxonomy	Closest placement reference	Closest genome ANI	Genome size (Mbp)	GC content (%)	CDS count	rRNA count
ID-0052	*Carnobacterium divergens*	GCF_000744255.1	98.91	2.65	35.1	2504	6
ID-0136	*Carnobacterium maltaromaticum*	GCF_000744945.1	99.70	3.59	34.5	3293	6
ID-1626	*Lactococcus carnosus*	GCF_006770265.1	96.53	2.36	38.7	2236	4
ID-0049	*Lactococcus raffinolactis*	GCF_001591765.1	89.88	2.14	42.1	2119	4
ID-0185	*Latilactobacillus curvatus*	GCF_004101845.1	98.00	2.11	41.7	2169	6
ID-0184	*Latilactobacillus sakei*	GCF_002370355.1	97.55	1.99	41.2	1967	7
ID-1609	*Leuconostoc gasicomitatum*	GCF_000196855.1	98.49	1.92	36.9	1911	4
ID-0467	*Leuconostoc mesenteroides*	GCF_000014445.1	98.81	2.07	37.7	2050	4
ID-0486	*Buttiauxella gaviniae*	GCF_001654835.1	98.60	5.12	49.5	4779	8
ID-1443	*Kluyvera intermedia*	GCF_900635475.1	98.74	4.62	52.6	4294	8
ID-1047	*Serratia liquefaciens*	GCF_000422085.1	98.19	5.41	55.3	4931	7
ID-1456	*Serratia proteamaculans*	GCF_946227095.1	98.81	5.57	55.0	5217	7
ID-0243	*Brochothrix thermosphacta*	GCF_000620985.1	99.04	2.60	36.5	2404	9

Table 2 | Fungal isolates and their classification based on BLAST® results

Internal ID	Closest genome taxonomy	Closest placement reference	Closest genome ANI	Genome size (Mbp)	GC content (%)	CDS count
ID-0367	*[Candida] zeylanoides*	GCA_031851675.1	91.10	10.63	55.4	6607
ID-0368	*Debaryomyces hansenii*	GCA_000006445.2	96.35	12.34	36.3	7487
ID-0991	*Debaryomyces hansenii*	GCA_000006445.2	95.93	12.16	36.4	6485
ID-1109	*[Candida] norvegica*	GCA_030567455.1	99.81	11.68	40.5	7372

monitored by measuring the optical density (OD) at 595 nm every 5 min. The results varied depending on the yeast-bacteria combination and supernatant concentration. *C. divergens* ID-0052 and *L. carnosus* ID-1626 exhibited significantly higher final OD values with three out of four yeast supernatants compared to fresh medium. Similarly, *L. sakei* ID-0184 displayed enhanced growth with three out of four yeast supernatants, but not with all concentrations. *Lactococcus* sp. ID-0049 was predominantly inhibited by the yeast supernatants, whereas the remaining LAB strains did not show significant responses. The results suggest that the yeast supernatants have the potential to enhance the growth of LAB, but the effect is strain-specific and influenced by both the yeast strain and the supernatant concentration. Additionally, the impact of LAB supernatants on the growth of *Serratia* and vice versa was tested (Supplementary Figs. 21–28). The results showed that the supernatants of the LAB effectively inhibited the growth of *Serratia*, as well as that of its own kin. The strength of inhibition depended on the concentration of the supernatant (Supplementary Fig. 27i). The supernatants of *Serratia* had different effects on the growth of the LAB: two strains, i.e., *L. sakei* and *Lactococcus* sp. ID-0049 showed interestingly shorter lag-phases in the presence of the *Serratia* supernatants, but the final ODs were lower compared to the control, while *C. maltaromaticum* had higher final ODs in the presence of the *Serratia* supernatants. We observed that LAB culture supernatants strongly inhibited the growth of *Serratia*. However, we assume that the inhibition is not solely due to the low pH, but rather a combination of organic acids and bacteriocins. Supporting this, *Serratia* was able to grow in acidified YPD medium (pH 4.6, comparable to the LAB supernatants), albeit with a prolonged lag phase (Supplementary Fig. 27i). Moreover, *Serratia* actively increased the pH of the surrounding medium, but only when it was not completely inhibited (Supplementary Fig. 29a, b). For example, even when initially exposed to acidic conditions (pH 4.6), *Serratia proteamaculans* raised the pH to around 6.7. None of the bacterial supernatants significantly impacted yeast growth (Supplementary Figs. 30– 33). Although yeasts, such as *Debaryomyces hansenii*, are described to increase environmental pH and thereby facilitate the growth of acid-sensitive bacteria[25], this pH-increasing effect was not observed in our experiments; [*C.*] *norvegica* even decreased the pH further (Supplementary Fig. 29i–l).

Genomic analysis on key taxa isolated from vacuum-packed beef points to biotic competition

Based on the results of the sequencing data and supported by the co-cultivation experiments, we hypothesized that LAB, Enterobacterales (particularly *Serratia*), and yeasts (particularly *Kurtzmaniella*) form a triangular interaction network, which is described in detail in the discussion section. The downstream analysis focused on potential mechanisms that could be involved in these interactions, i.e., secondary metabolite clusters, secretion systems, extracellular enzymes, and metabolic capabilities. The interaction mechanisms are diverse; therefore, this paper focused only on a selection of frequently described examples.

In order to describe possible inhibitory mechanisms of LAB over Enterobacterales, the potential formation of secondary metabolites (e.g., bacteriocins) and the formation of organic acids were investigated. Briefly, the analysis of secondary metabolite gene clusters revealed that some LAB strains may effectively inhibit the growth of other bacteria (Supplementary Table 11). *C. maltaromaticum* demonstrated the potential to produce leucocinA/sakacin P family class II bacteriocins and radical SAM proteins. Similarly, *L. gasicomatitum* could produce class II bacteriocins, and *L. carnosus* exhibited the potential to produce radical SAM/SPASM proteins and type 2 lanthipeptide synthetase. According to the genome-scale metabolic models (GEMs) generated with CarveMe, all LAB strains could produce L-lactate, acetate, formate, succinate, and L-malate. Further, five out of the seven LAB strains could produce D-lactate, and six of them also produced citrate (Supplementary Table 12).

Enterobacteriaceae harbored several siderophores (e.g., aerobactin, enterobactin), homoserine lactone synthase (*S. proteamaculans*), non-ribosomal peptide synthetase (NRPS, *S. liquefaciens* and *S. proteamaculans*), and β-lactone synthase genes (Supplementary Table 13). In addition, multiple genes potentially involved in acid stress resistance, including pyruvate formate lyase[26], the arginine deiminase system[27], glutamate

dehydrogenase, and glutaminase were detected. Three Enterobacterales strains (i.e., *S. liquefaciens*, *S. proteamaculans*, and *B. gaviniae*) exhibited the potential to harbor a type IV secretion system. *B. gaviniae* additionally possesses the genes for contact-independent type I and type II secretion systems. *K. intermedia* demonstrated the potential to produce a contact-dependent type VI secretion system. These strains can also produce serine and metalloproteases (e.g., PrtC and PrtS, which were only produced by *S. proteamaculans*) and chitinase (EC 3.2.1.14). However, they lacked genes to degrade 1,3-β-glucans (i.e. EC 3.2.1.39, EC 3.2.1.58). Further, the GEMs were searched for compounds that were described as VOCs with potential antifungal activity (Supplementary Table 14). The Enterobacterales strains could produce ammonia, hydrogen cyanide, methanethiol, ethanol, and isovaleric acid.

Within the yeasts' genomes, we searched for enzymes that are potentially capable of breaking down more complex organic molecules and making them available to the bacterial community, particularly the LAB community. According to the KEGG results, each examined yeast contained a set of acyl glycerol hydrolases (EC 3.1.1.3), while none of the sequenced bacteria did. The presence of TAG (TGL2, TGL3, TGL4) and acylglycerol lipases (EC 3.1.1.23) in the yeast genomes suggests their potential to mobilize and process triglycerides and other complex lipids. The presence of multiple aspartic endopeptidases and a metalloprotease in our yeast genomes suggests a significant role in protein degradation and potential cross-feeding interactions with bacterial communities. Notably, the detection of EC 3.4.23.24 (secreted aspartyl protease, candidapepsin) indicates that yeasts actively degrade extracellular proteins, releasing peptides that could be utilized by bacteria.

Discussion

The use of 16 S and 18 S rRNA gene amplicon sequencing data paired with spike-in cells and qPCR in this study allowed a description of the growth curves of individual ASVs, species, and genera. This approach provides a more accurate description of microbial dynamics compared to traditional relative abundance semi-quantification methods, enables the tracking of microbial growth and offers a clearer view of actual biological shifts. By capturing actual population dynamics rather than compositional shifts, this method provides stronger evidence for microbial interactions, competition, and potential functional contributions. It should be noted that amplicon sequencing, as performed in this study, also detects non-viable cells. However, the longitudinal setting also shows that many of the abundant taxa exhibit active growth and, for the most part, could also be cultivated.

The microbial successions we observed were consistent with those reported in previous studies on comparable samples. For instance, *Psychrobacter*, *Acinetobacter*, *Pseudomonas*, and *Moraxella* were found in highly relative abundances on day 0 of sampling in beef production[14,15]. Our data show that *Pseudomonas* and *Brochothrix* reach their growth plateau by day 6, but contrary to compositional sequencing data, they remain present and presumably alive after 85 days. It can be assumed that they grow initially after vacuum-packaging due to the presence of residual oxygen, but subsequently exhibit minimal growth. A small but detectable proliferation in the absence of oxygen has been described for *Pseudomonas fragi*, *P. lundensis*, and *P. weihenstephanensis*[28]. Most of LAB, as well as the majority of Enterobacterales, reached their growth plateau after around 2 weeks. The increase in LAB, which constitute around 75% of the total bacterial population on day 15, is ultimately accompanied by a massive reduction in alpha diversity as they significantly dominate the microbiota, which goes in line with previous studies[17,29,30]. Until now, the growth of bacteria on meat has mainly been described using specific culture media, which often quantify entire genera or groups with similar environmental requirements. The advantage of using spike-in cells, coupled with taxonomic marker genes amplicon sequencing, allows a more precise description of the dynamics of individual taxa. It is interesting in this context that all dominant ASVs (amplicon-defined taxa) reached their population maximum well before the best-before date of the tested product (day 55). This observation reinforces that bacterial numbers per se are not necessarily indicative of spoilage, and that the accumulation of microbial metabolic products is ultimately decisive in determining product quality[15,29]. It should be mentioned here that the products were not explicitly tested for spoilage. The role of lactic acid bacteria (LAB) in meat spoilage is multifaceted and context-dependent, as they are both associated with protective effects (through acidification and competitive exclusion) and spoilage activity (via the production of undesirable metabolites)[7]. *Carnobacterium* and *Leuconostoc* were the primary contributors (or at least mostly described) to the production of volatile organic compounds (VOCs) associated with spoilage[13]. These genera are known for their ability to metabolize sugars and amino acids into compounds such as alcohols, aldehydes, ketones, esters, volatile fatty acids, and sulfur compounds, which can impact the sensory quality of meat[13]. Jääskeläinen et al. compared vacuum-packed beef with high-oxygen modified atmosphere-packed (MAP) beef and showed that MAP beef spoiled 10 days earlier than the VP beef, and showed higher populations of *Leuconostoc*, while in VP, *Lactococcus* and *Lactobacillus* were dominant[17]. This is particularly interesting considering that *Carnobacterium divergens* and *Leuconostoc gasicomitatum* appear to be the most substantial benefactors of the fungal populations, while *Carnobacterium maltaromaticum* and *L. gasicomitatum* are potential inhibitors against other spoilers such as *Serratia*. Apart from the LAB, *Serratia* has the largest population in the bacterial community in matured meat, and it has been described that they can contribute significantly to spoilage with their metabolic products[13]. Interestingly, bacteria that are traditionally considered relevant meat spoilers, such as *Pseudomonas* and *Brochothrix*, were not detected in high numbers on the meat surface[10,13]. However, their mere absence from dominant growth patterns does not necessarily mean they are irrelevant for spoilage. Our data suggest that these species persist at subdominant levels (~10^5 CFU g^{-1} in some samples) while remaining metabolically active, potentially contributing to spoilage through the production of VOCs. This supports the idea that spoilage is not solely a function of bacterial abundance but rather of metabolic activity and accumulation of specific spoilage compounds[29]. Taken together, these findings highlight the need to consider both abundant and low-abundance taxa when assessing microbial contributions to meat spoilage, as even bacteria that remain at low cell densities may still play a functional role in odor development and overall meat quality deterioration[31]. However, the cultures carried out in parallel with the molecular biological methods, which were primarily intended to obtain isolates for downstream experiments, did not cover the entire spectrum of the microbial community. Psychrotrophic bacteria and strict anaerobes were not considered. However, the information obtained from amplicon sequencing made it possible to provide taxon-targeted media and conditions from the reserve samples as needed to enable isolation of the desired taxon, as was done for *Psychrobacter*, for example.

The fungal population maintained its alpha diversity through time and was dominated by [*C.*] *zeylanoides* (*Kurtzmaniella*), which is present in all samples and reached its maximum population after around 30 days. Other genera, such as *Barnettozyma*, *Debaryomyces*, and *Yarrowia*, showed a similar pattern. The fungal population in batch 3, however, appears less stable and showed 9 - 16 times smaller *Kurtzmaniella* populations compared to batches 1 and 2. Comparing the bacterial and fungal sequencing data raises the question of whether the presence of *Serratia* and other Enterobacterales (i.e., *Kluyvera*, *Butauxiella*) in batch 3 may have influenced the fungal population, particularly *Kurtzmaniella*. The network analysis revealed that *Kurtzmaniella* and *Barnettozyma* are directly associated with several highly abundant LAB, as well as with a *Brochothrix* and a *Serratia proteomaculans* strain. Furthermore, many of the higher-abundant bacterial species are indirectly (second-order) associated with these yeasts, among them *Serratia* and *Kluyvera*. The co-culture and cell-free supernatant experiments showed that the presence of yeasts can have a positive effect (i.e., increased growth rate or increased carrying capacity) on the LAB, but little to no effect on the examined Enterobacterales (Fig. 2c). The yeasts, however, are negatively affected by both groups, but four times more strongly by the Enterobacterales.

Based on the results of this study, we raise the question of whether yeasts, LAB, and enterobacteria interact in a triangular relationship (Fig. 2d), consisting of three axes of mutually modulating pairwise interactions. The first axis represents the interaction between LAB and yeasts. Co-culture experiments demonstrated that the presence of yeasts can positively influence LAB growth, likely due to yeast-derived metabolites beneficial to LAB. This hypothesis is supported by cell-free supernatant experiments, which showed that yeast supernatants can enhance the growth of certain LAB strains. Notably, both experiments were conducted in a medium already containing yeast extract, suggesting that the yeasts produce additional metabolites that further promote LAB growth. Particularly, the cross-feeding of amino acids provided by yeasts to LAB has been described in previous studies[32,33]. We assume that this effect is even stronger on meat, since the yeasts have a broader range of enzymes to degrade complex proteins and fats, which are present in meat, i.e., lipases, and proteases[34–36]. While the bacterial genomes lacked EC 3.1.1.3 lipases, yeast activity could release free fatty acids and glycerol, which are more easily utilized by bacteria. Čanak et al. described a cold-active lipase from [*C.*] *zeylanoides* which has an optimum at 27 °C, but still has 60% of its activity at 7 °C[37]. In general, *D. hansenii*, [*C.*] *zeylanoides*, and *Yarrowia lipolytica*, which is also present in the sequencing data, are associated with lipolytic and proteolytic activities[38–40]. In particular, the presence of genes for EC 3.4.23.24 (secreted aspartyl protease) suggests an extracellular proteolytic activity that can benefit the bacteria, especially since they are described to function over a broad pH range (~2–7)[41].

Another described effect of yeasts is that they can increase the pH of the environment[42], which consequently positively impacts bacterial growth. However, in our study, yeasts did not exhibit this pH-modulating effect. Instead, they contributed to a pH decrease in the medium. This suggests that yeast-derived metabolites, rather than pH modulation, play a key role in LAB growth enhancement. In the opposite direction of this interaction, LAB inhibited yeast growth under these experimental conditions. However, the effect of the LAB supernatants on the yeasts was weaker, suggesting that direct microbial interactions rather than secreted metabolites may drive this effect. Notably, the inhibitory effects of LAB on yeasts have been described and are also desirable in foods as they delay yeast-induced spoilage[43].

The second axis represents the interactions between the LAB and the Enterobacterales, particularly *Serratia*. Many LAB are known for their antimicrobial properties, which are mainly based on the production of organic acids and bacteriocins[44]. Another often used explanation is the strong acidification of the environment by LAB[45]. Although we see in the supernatant experiments that a reduced pH of fresh medium delays the growth of the tested Enterobacterales, the effect is significantly weaker than when using cell-free LAB supernatants. In fact, we see that *Serratia* can raise the *pH* values of the supernatants, provided that it remains viable and continues to grow. As the reduced *pH* value in this context is mainly caused by organic acids, it should be mentioned that all tested Enterobacterales possessed genes for a potential organic acid resistance (i.e., pyruvate formate lyase). Furthermore, all examined Enterobacterales had genes for enzymes that metabolize L-lactate anaerobically to pyruvate, followed by its further conversion to either formate or acetate. All strains harbored genes for glutamate dehydrogenase and glutaminase, which are important enzymes for producing ammonia. Further, two strains had genes for the whole arginine deiminase pathway (arcABC), and the arginine ornithine antiporter (arcD), which is an important system for acid tolerance and ATP generation, particularly under anaerobic or energy-limited conditions[46,47]. Genomic potential suggests that these strains may contribute to pH neutralization in their environment. Consequently, we assume that the production of organic acids by LAB alone may be insufficient to inhibit the growth of certain Enterobacterales, which might explain the persistence of *Serratia* in some samples throughout the examination period. In addition to pH and organic acids, bacteriocins may also play a role in inhibiting *Serratia*. In this study, we detected the potential for bacteriocin production in *C. maltaromaticum*, *L. gasicomitatum*, and *L. carnosus*. While our study does not yet clarify whether the observed inhibition is driven by pH, organic acids, or bacteriocins, it is possible that a combination of these factors is involved. Notably, inhibition of *Serratia* and other bacteria by *C. maltaromaticum*, also isolated from beef, was previously demonstrated by Zhang et al.[48].

The third axis is the interaction between yeasts and *Serratia*. The co-culture experiments showed that the presence of Enterobacterales, particularly *Serratia proteomaculans* ID-1456, has a strong adverse effect on the growth of the yeasts. The amplicon sequencing data also support this, since the presence of *Serratia* and other Enterobacterales is negatively correlated with the presence and number of yeasts. The whole genome sequencing data revealed that *S. proteomaculans* has the potential to produce several chitinases, extracellular proteases (PrtC, PrtS), and exo-1,3-β-glucanases, among other enzymes, which are necessary for fungal cell wall degradation[49]. However, they lack endo-1,3-β-glucanases, which are essential for efficient fungal cell wall degradation[50]. Additionally, *S. proteomaculans* harbors type IV secretion system genes, which are required to inject effector proteins into eukaryotic cells[51,52]. However, the described interaction mechanisms between *Serratia* and fungi are mainly based on *Serratia marcescens* and are usually based on type VI secretion system[53], which is not present in the isolated *Serratia* strains. Apart from this, there are several other potential explanations for the inhibition of the fungi by *Serratia*. Commonly reported factors include siderophores, haterumalides, prodigiosin, Tfe1 and Tfe2, volatile organic compounds (VOC)[53–58]. Carter-House et al. tested the effect of *S. marcescens*, *S. proteamaculans* and *Bacillus subtilis* on the growth of *Rhizopus stolonifer* and described *S. proteamaculans* as the most effective inhibitor of the fungi[59]. Within this study, they tested three volatiles (i.e. 2-undecanone (*B. subtilis*), anisole (*S. marcescens*), and dimethyl trisulfide (*S. proteamaculans*)) and found that all three of them are able to inhibit the growth of the fungi. However, none of these volatiles were found in the GEMs of the tested *Serratia* strains. On the other hand, if inhibition were mediated by volatiles, we would have expected the cell-free supernatants of the *Serratia* strains to inhibit yeast growth. The lack of such an effect may indicate a different mechanism, or that active compounds were unstable or degraded under the tested conditions. The relationship between *Serratia* and the yeasts requires further study. However, the current data indicate that this axis exists. We hypothesize that this interaction may have significant implications for the composition of the community colonizing meat. Specifically, the negative impact on the yeast population may disrupt the fungi-LAB interactions axis, potentially weakening the inhibitory function of LAB on other bacteria, especially Enterobacterales. However, the simplified experimental setting does not reflect the complexity of real-world microbial dynamics on meat. This is impossible due to the different biochemical composition of meat and the medium used, the different bioavailability of nutrients, and, above all, the reduction of the microbial community. Nevertheless, simplified experiments such as these are the first step toward understanding interactions. Our results suggest a dynamic 'triangle of interactions' between LAB, yeasts, and Enterobacterales. While this conceptual model is grounded in robust observational data, additional validation through targeted experiments, such as metabolite tracing or controlled co-cultivation studies, is necessary to elucidate mechanisms driving these interactions. It is also important to acknowledge that LAB have a dual role in vacuum-packed meat. They may inhibit spoilage organisms through acidification and antimicrobial activity, but can also contribute to spoilage via the production of volatile metabolites.

Towards developing practical applications, our study provides a foundation for microbiome-informed strategies to improve meat preservation. For example, the identification of yeast-derived metabolites that enhance LAB growth could lead to the development of yeast-based additives or starter cultures to promote beneficial LAB activities while suppressing spoilage organisms. Additionally, the inhibitory effects of LAB on Enterobacterales suggest that LAB strains with strong antimicrobial properties could be selectively introduced into packaging systems to reduce spoilage risks. Furthermore, the discovery of fungal cell wall-degrading enzymes produced by Enterobacterales highlights the potential for targeted interventions to mitigate their negative impact on yeasts, thereby preserving the positive LAB-yeast interactions. These insights inform the design of tailored

microbial consortia or bioprotective cultures for vacuum-packed meat in the future. Our findings also suggest that monitoring microbial interactions, rather than focusing solely on individual taxa, could improve quality control measures in the meat industry. For instance, the detection of specific microbial interaction patterns, such as the triangular interaction network, could serve as an early indicator of spoilage risk, enabling more precise interventions. This approach represents a shift from traditional spoilage detection methods to a more dynamic, systems-based understanding of microbial communities in meat packaging. Future research should focus on validating our findings under real-world conditions, such as in commercial meat packaging environments, and exploring the metabolic pathways and signaling molecules involved in these interactions. A deeper understanding of these mechanisms will enable the development of more precise and effective strategies for controlling spoilage and improving meat quality.

Methods

Sample collection

All striploins (boneless), which predominantly consist of the *Musculus longissimus dorsi*, were sourced from young bulls slaughtered at the same commercial facility, which includes both a slaughterhouse and a cutting plant. Animals were processed on three different days, one batch per week, but all processing steps were performed under comparable hygienic conditions. Slaughter occurred 2 days prior to the start of the sampling period, and each striploin weighed ~1.5–2.0 kg. A total of three batches were sampled, with each batch containing three striploins.

After cutting at the facility, the striploins were transported on ice to our institute for further processing, which began promptly upon arrival. To ensure sample homogeneity and consistent analysis, each striploin was cut into 12 equally sized slices (~120–150 g each) using sterile tools. The first slice was processed immediately, while the remaining 11 slices were individually vacuum-packed in sterile vacuum-packed in 200 × 300 mm vacuum bags (la.va, Landig + Lava GmbH & Co.KG, Bad Saulgau, Germany) using a V350® vacuum sealer (la.va) and stored at 4–6 °C for 3, 6, 9, 15, 28, 41, 55, 70, and 85 days, respectively.

Meat preparation

While sponge sampling is commonly used for surface hygiene testing, we opted to excise a thin (~3 mm) layer of the meat surface to ensure effective recovery of microbial communities from both the outer and near-surface layers, especially after extended storage times. This approach aimed to increase consistency and microbial yield across samples, despite the higher content of host DNA. Approximately 25 g of the original surface of each striploin slice was cut off using sterile tweezers and scalpels and homogenized in sterile Stomacher® bags (Seward Ltd, Worthing, United Kingdom) with 1:10 (w/v) 1 × phosphate-buffered saline (PBS, Gibco, Bleiswijk, The Netherlands) for 2 min with 4 beats per second using a BagMixer® 400 CC (Interscience, Puycapel, France). Two 15 ml aliquots of each homogenate were centrifuged for 10 min at 4 °C and 4000 × rcf in an Eppendorf Centrifuge 5810R (Eppendorf Corporate, Hamburg, Germany) equipped with an A-4-62 rotor (Eppendorf Corporate). The resulting pellets were resuspended in 2 ml of 1 × PBS and stored at −80 °C until further processing.

A portion of the homogenate was mixed with 50% glycerol at a 1:2 (v/v) ratio and frozen at −80 °C for subsequent recultivation. The remaining homogenate was used immediately for the cultivation procedure.

Cultivation

Each homogenate was diluted 1:10 in 1 × PBS. For each dilution step, 100 µl of each dilution were plated on various agar media following the recommended cultivation conditions. To cultivate bacteria, 100 µl of each dilution was plated on Plate Count Agar (PCA, Biokar Diagnostics, Allonne, France) and De-Man-Rogosa-Sharpe agar (MRS, Oxoid, Basingstoke, UK). Both media were incubated aerobically at 30 °C for 48 h. Additionally, 100 µl of each dilution was plated on Violet Red Bile Glucose agar (VRBG, Biokar Diagnostics, Allone, France) and incubated aerobically at 37 °C for 24 h. Although ISO methods recommend pour plating with 1 mL inoculum for this medium, we used 100 µL surface spreading to enable consistent isolation across all media types, as our aim was not quantitative enumeration for food safety purposes but rather strain isolation.

For fungal cultivation, 100 µl of each dilution was plated on Rose Bengal chloramphenicol agar (Biokar Diagnostics) and incubated aerobically at 25 °C for 5 days. Two plates of Yeast Glucose Chloramphenicol Agar (YGC, 0.5% yeast extract (micro-granulated, Roth, Karlsruhe, Germany), 2% D(+)-glucose (Roth), 0.01% chloramphenicol (Carl Roth GmbH, Karlsruhe, Germany), 1.8% bacteriological agar type E (Biokar Diagnostics)) were also used for each dilution, with one incubated at 25 °C for 5 days and the other at 4 °C for 10 days. Media and solvent quality controls were included in each experiment.

All cultivations were performed under aerobic conditions to streamline isolation and recovery. This decision was based on the expectation that many of the dominant taxa would be aerotolerant or facultatively anaerobic, and that strict anaerobes could still be identified via parallel amplicon sequencing.

After incubation, colonies were counted, and the colony-forming units (CFU) per gram of meat were calculated. Morphologically distinct colonies were picked from each medium, at each sampling point and from each batch, and re-streaked to obtain pure cultures for subsequent identification.

In addition to the standard cultivation methods described above, an additional cultivation round was performed to specifically isolate *Psychrobacter*, a taxon that was highly abundant in the early stages of meat storage. For this purpose, backup frozen cell pellets from the two samples with the highest relative abundances of *Psychrobacter* were thawed, serially diluted, and plated on Marine Agar (marine broth (Roth) + 1.5% bacteriological agar type E). Plates were incubated at 20 °C for 72 h. This targeted approach allowed for the successful isolation of *Psychrobacter*, providing isolates for potential downstream experiments.

Sanger sequencing and isolate classification

DNA was extracted from pure cultures using a protocol modified from Walsh et al.[60] for PCR-based identification. For this study, 100 µl of 0.01 M TRIS/HCl (Trizma® base, Sigma-Aldrich, St. Louis, United States) and 400 µl of a 2.5% Chelex® 100 Resin solution (BioRad, Hercules, United States) were used to lyse cells at 95 °C for 10 min. After centrifugation at 13,000 × rcf for 30 seconds, the supernatants were used for 16 S or 18 S rRNA gene amplification with universal primers.

For 16S rRNA gene PCR the primers 27F (5'-GAG TTT GAT C**M**T GGC TCA G-3') and 1492R (5'-GG**Y** TAC CTT GTT ACG ACT T-3') were used. The reaction mix contained 0.025 U/µl Platinum™ Taq DNA Polymerase (Invitrogen™, Vilnius, Lithuania), 1 × TaqMan PCR buffer, 2 mM $MgCl_2$, and 250 nM dNTP Mix (Thermo Scientific™, Vilnius, Lithuania) and 200 nM of each primer. The thermal cycling protocol consisted of an initial activation at 95 °C for 5 min, followed by 35 cycles of 40 seconds at 95 °C (denaturation), 40 s at 52 °C (annealing), and 1 min at 72 °C (elongation). Negative extraction and PCR controls were included, and *Lacticaseibacillus rhamnosus* (NCTC 10302) DNA served as a positive control. PCR products were analyzed using a QIAxcel DNA Fast Analysis Kit on a QIAxcel Advanced instrument and the QIAxel ScreenGel Software version 1.6.0 (Qiagen, Hilden, Germany).

For 18S rRNA gene amplification the primers Euk528F (5'-CGG TAA TTC CAG CTC C-3') and U1391R (5'-GGG CGG TGT GTA CAA **R**G**R**-3')[61] were used. The reaction mix and thermal cycling conditions were the same as those for the 16S rRNA gene PCR, except for setting the annealing temperature to 56 °C.

Cultures that were negative in both 16 S and 18 S rRNA gene PCR underwent a second DNA extraction using the NucleoSpin Tissue Kit (Macherey-Nagel, Düren, Germany), following the support protocol for hard-to-lyse bacteria.

PCR products were purified and sequenced in one direction by LGC Genomics GmbH (Berlin, Germany), using the 27F primer for 16 S rRNA and the Euk528F primer for 18 S rRNA gene amplicons.

The processing of the Sanger sequences was conducted in R (v. 4.4.1)[62] using a workflow that incorporated quality trimming, taxonomic classification, clustering, and phylogenetic tree construction. Sanger sequences were trimmed using the "SangerRead" function from the `sangeranalyseR` package (v. 1.16.0)[63]. The trimming was based on the "M2" method, with a quality score cutoff of 35 and a sliding window size of 15. Bacterial sequences were classified using the "assignTaxonomy" function from the `DADA2` package (v1.34.0)[64], and the SILVA (release 138.2)[65], GTDB (release 220)[66], and RefSeq+RDP (v16)[66] databases. Fungal sequences were classified using a pretrained classifier generated from the SILVA database (release 138.2), employing modified code from McLaren[67]. Only sequences with a minimum bootstrap confidence of 100 were initially classified. Sequences longer than 100 bp were retained for further analysis. Classifications with consistent matches across all three databases (or two matching and one unclassified) were included in the main analysis. Sequences with lower confidence scores (minimum bootstrap confidence of 90) or inconsistencies were separately documented (Supplementary Tables 1–3). Sequences longer than 1000 bp for bacteria or 900 bp for fungi were clustered using the "Clusterize" function from the `DECIPHER` package (v. 3.2.0)[68], with a cutoff of 0.001 to group sequences by similarity. For each genus, the sequence from the most prevalent cluster with the greatest length was selected as the representative sequence. Representative sequences were aligned using `msa` package (v. 1.38.0)[69] in combination with the multiple sequence alignment algorithm MUSCLE[70]. The alignments were refined with `Gblocks` (v. 0.91b)[71] to remove poorly aligned regions and gaps. Phylogenetic trees were constructed using the "TreeLine" function from the `DECIPHER` package, with a default setting for clustering and tree construction. Using the `ggtree` (v.3.14.0)[72] and `phylobase` (v.0.8.12)[73] packages, tree visualization was created with additional layers showing diversity, isolation time points, and batch presence for each genus (Supplementary Fig. 7). Additionally, the sequences were used to create a BLAST database, which was used to match the isolates with the sequences obtained from the 16 S and 18 S rRNA gene amplicon sequencing.

Whole genome sequencing and processing

For the whole genome sequencing thirteen bacterial and four yeast strains were selected and cultured in YPD medium (1% yeast extract, 2% peptone (tryptic digest, Roth), 2% D(+)-glucose) at 25 °C for 48 h under permanent shaking (125 × rpm, Heidolph Unimax 1010, Schwabach, Germany). The cultures were harvested for 10 min at 8000 × rcf. The pellets were used for DNA extraction using Monarch™ High Molecular Weight DNA Extraction Kit (New England Biolabs Inc., Ipswich MA, US). For the bacteria, the protocol "Bacteria gDNA extraction for Nanopore-only microbial Isolate Sequencing Solution (NO-MISS) - Rapid Barcoding Kit V14 (SQK-RBK114.24)" suggested by Nanopore[74], and for the fungi the protocol "Fungi gDNA extraction for Nanopore-only Microbial Isolate Sequencing Solution (NO-MISS) - Rapid Barcoding Kit V14 (SQK-RBK114.24)"[75] was used with small modifications. The bacterial pellet was resuspended in 100 μl lysozyme (25 mg ml^{-1}) from chicken egg white (Sigma-Aldrich, solved in TE-buffer pH 8.0 (10 mM TRIS Pufferan® (Carl Roth GmbH + Co. KG, Karlsruhe, Germany), 1 mM EDTA (Sigma-Aldrich)). The Monarch™ gDNA elution buffer was preheated to 70 °C instead of 60 °C. For the last step, bacterial DNA was eluted in a 40 μl gDNA elution buffer. Broth cultures were centrifugated for 10 min at 8000 × rcf. For the fungal pellet instead of metapolyzyme, as recommended by Oxford Nanopore, Zymolyase Ultra enzyme (50U per sample, Zymo Research, Irvine, US) was used. Zymolyase was prepared by reconstituting it in TE buffer to 50U per sample. The incubation at 37 °C for 45 min was extended to 90 min if the lysis was incomplete. Similar to the modified bacterial protocol, the Monarch™ gDNA elution buffer was preheated to 70 °C instead of 60 °C. The fungal DNA was removed from the beads and eluted finally in 20 μl in gDNA elution buffer. The DNA concentration of eluted samples was determined by a Qubit® 2.0 Fluorometer (Invitrogen™, Vilnius, Lithuania) using the Qubit® dsDNA BR Assay Kit (Invitrogen™). Additionally, to assess the integrity, quality, and quantity of the isolated gDNA, the Genomic DNA ScreenTape assay (Agilent Technologies Österreich GmbH, Vienna, Austria) within the Agilent 4200 TapeStation system (Agilent Technologies, Santa Clara, US) and software revision A.02.02 (SR1) was used. The DNA was stored at −20 °C until further processing. The DNA was prepared for sequencing using the Rapid Barcoding Kit V14 (SQK-RBK114.24, Oxford Nanopore Technologies, Oxford, UK) using Protocol ISO_9205_-v114_revC_30Sept2024 for MinION[76]. The sequencing was done on a MinION Mk1B (Oxford Nanopore Technologies) device using the MINION Flow Cells (FLO-MIN106D, Oxford Nanopore Technologies). Each sequencing was done for 72 h using the MinKNOW™ software (v. 24.06.16, Oxford Nanopore Technologies).

The basecalling, using model dna_r10.4.1_e8.2400bps_sup@v.5.0.0 and the demultiplexing was done with `dorado` (v. 0.8.3)[77]. The reads were then filtered for a min length of 1000 bp and a min mean quality of 9 using `filtlong` (v. 0.2.1)[78]. The assembly was done using three iterations of `flye` (v. 2.9.5)[79]. The downstream procedure differed for bacteria and yeasts. The assembly of the bacteria was followed by a polishing using `medaka` (v. 2.0.1)[80]. The quality of the assemblies was checked using `checkm` (v. 1.2.3)[81], followed by taxonomy classification using the `GTDB-tk` (v. 2.4.0)[82,83], and annotation using `prokka` (v. 1.14.6)[84]. The assemblies of the yeasts were polished using four repetitions of `racon` (v. 1.5.0)[85] followed by one round of polishing with `medaka`. The assembled contigs were initially classified using `Kraken2` (v. 2.1.3)[86]. Contigs classified as bacteria (i.e. all contigs classified as bacteria were classified as *Lactococcus raffinolactis*, which was sequenced on the same flow cell), had a different GC content compared to the contigs of interest and a lower coverage, and were consequently removed before the next steps (Supplementary Fig. 34). The remaining contigs were classified again using BLAST®(v. 2.16.0)[87] in combination with a fungal specific database generated from eukaryote nucleotide NCBI database. `Busco` (v. 5.8.2)[88] was used to check the assemblies for the presence of specific orthologs (used reference: Saccharomycetes) to estimate the completeness of the assemblies, which was done before and after the removal of the bacterial contigs. To further refine species classification, we performed `FastANI` (v. 1.34)[89] analysis on our final genome assemblies. As reference genomes, we selected publicly available sequences from species that exhibited the highest sequence similarity in our initial BLAST®-based classification. For annotation the web-based version of `Companion` (v. 2.2.12)[90] was used. For bacteria and yeasts secondary metabolite gene clusters were predicted using `antiSMASH` (v. 7.1.0)[91]. Further, `EggNOG-mapper` (v. 2.1.12)[92,93] in combination with the Kyoto Encyclopedia of Genes and Genomes (KEGG)[94] was used to predict the presence of secretion systems, extracellular enzymes, and metabolic capabilities, and `dbCAN3` (v. 4.1.4)[95] to predict carbohydrate-active enzymes. `CarveMe` (v. 1.6.2)[96] was used to predict the metabolic capabilities of the bacterial isolates. The generated GEMs (Genome-scale Metabolic Models) were used to predict the production of organic acids and volatile organic compounds (VOCs).

Cell pellet preparation, DNA extraction, amplicon sequencing and processing

Prior to DNA extraction the frozen cell pellets were thawed on ice, and centrifuged (16,000 × rcf, 10 min at 4 °C) using an Eppendorf Centrifuge 5810R and an A-4-62 rotor. After removal of the supernatant, the pellets weighting >0.5 g was split to avoid overloading the subsequent lysis procedure. Before adding 450 μl of pre-heated (55 °C) MBL buffer from the DNeasy® PowerFood® Microbial Kit (Qiagen), 20 μl of ZymoBIOMICS Spike-in Control I (High Microbial Load, ZymoResearch) was added. The spike-in was diluted to 1:4000 in MBL buffer (10^4 cells) for samples with a ripening duration of 0–9 days and 1:40 (10^6 cells) for samples with a ripening duration of 15–85 days, ensuring a final concentration of 0.1–10%. This dilution strategy was chosen to maintain a detectable range for the spike-in across varying microbial loads. Spike-in controls are an established method for estimating absolute microbial abundances in amplicon sequencing workflows[97–99]. The pellets resuspended in MBL buffer were transferred to the provided lysis tubes and processed according to the DNeasy®

PowerFood® Microbial Kit Handbook[100]. The DNA concentration was determined by the Qubit® 2.0 Fluorometer (Invitrogen™, Vilnius, Lithuania) using the Qubit® dsDNA BR Assay Kit (Invitrogen™). The presence of 16 S rRNA gene DNA was checked by the 16 S rRNA gene PCR, as described for the isolates, followed by the analysis of the PCR products with a QIAxcel DNA Fast Analysis Kit (Qiagen) in a QIAxcel Advanced system (Qiagen). The extracted DNA was stored at −20 °C until further processing. A total of 110 samples, two ZymoBIOMICS Microbial Community Standards (Zymo Research), and 18 negative controls were included in the library preparation and amplicon sequencing. The generation of the 16 S and 18 S rRNA gene amplicon library, as well as the sequencing was carried out at Baseclear B.V. (Leiden, The Netherlands) using the Illumina MiSeq PE300 system. The V3-V4 region of the 16S rRNA gene was amplified using the primers 341F (5'-CCT ACG GG**N** GGC **W**GC AG-3') and 805R (5'-GAC TAC **HV**G GGT ATC TAA TCC-3'), as described by Klindworth et al.[101] along with Illumina adapter sequences (5'-CGT CGG CAG CGT CAG ATG TGT ATA AGA GAC AG-3' and 5'-GTC TCG TGG GCT CGG AGA TGT GTA TAA GAG ACA G-3', respectively). For the amplicon sequencing of fungal 18S rRNA genes, we used the primer 574*f (5'-CGG TAA **Y**TC CAG CTC **YV**-3', described by Hugerth et al., 2014[102]) as the forward primer, and a modified fungi-specific reverse primer (5' -AGA CTA C**N**A CGG TAT CT**R**- 3', originally described as a forward primer by Vainio and Hantula, 2000[103]). This primer pair targeted the V4 region of the 18S rRNA gene, generating an amplicon of 445 bp in length. To assess primer specificity, we conducted an in silico analysis using the PR2 database (v. 5.0.1)[104], which revealed a coverage of 88% for fungal species and 91–100% for yeast species, while demonstrating no amplification of *Bos taurus* DNA. Further, we validated the primers in vitro via PCR using meat samples and yeast isolates from this study. The PCR master mix consisted of 0.025 U μl^{-1} Platinum™ (Invitrogen™), 1 × TaqMan PCR buffer, 2 mM $MgCl_2$, 250 nM dNTP Mix (Thermo Scientific™), and 400 nM of each primer. The thermal cycling conditions included an initial activation step at 95 °C for 5 min, followed by 35 cycles of denaturation (95 °C, 40s), annealing (46 °C, 40s), and elongation (72 °C, 1 min). The same conditions were subsequently used by BaseClear B.V. for amplicon sequencing.

The following steps were performed by BaseClear B.V. The FASTQ sequence files were generated using bcl2fastq version 2.20, which converted the raw base call files into FASTQ format. An initial quality assessment was performed on data passing the Illumina Chastitiy filtering. Subsequently, reads containing PhiX control signal were removed using an in-house filtering protocol. In addition, reads containing (partial) adapters were clipped (up to a minimum read length of 50 bp). The second quality assessment was based on the remaining reads using the FASTQC quality control tool version 0.11.8.

Following the preprocessing steps by BaseClear B.V., we processed the raw paired-end sequence reads for both the 16S and 18S datasets. The reads were initially evaluated for quality using `FastQC` (v. 0.11.9)[105], followed by adapter trimming with `Trimmomatic` (v. 0.39)[106]. Post-trimming quality was reassessed using `FastQC` and summarized with `MultiQC` (v. 1.13)[107]. The further downstream processing and analysis were preformed using `QIIME2` (v2024.2.0)[108]. Sequencing data were imported into `QIIME2` in `Casava` 1.8 paired-end demultiplexed format. Quality profiles were generated to determine optimal truncation lengths. Denoising, chimera removal, and merging of paired-end reads were conducted using the `DADA2` plugin[64]. Truncation lengths were set to 270 bp (forward) and 210 bp (reverse) for both 16S and 18S datasets. Multiple parameter combinations were tested for `DADA2` trimming, with the final selections based on trimming efficiency and retention of high-quality reads. Taxonomy was assigned using the q2-feature-classifier plugin and the Scikit-learn algorithm with pre-trained classifiers from the SILVA 138.1 database (16S)[109] and SILVA 138 database (18S)[110]. Contaminant sequences, including chloroplasts, mitochondria, and unassigned taxa, were removed. Specific mitochondrial sequences of *Bos taurus* and *Homo sapiens* were filtered using BLAST® against reference genomes. For the 16 S dataset, contaminants were identified and removed using R and the package `decontam` (v. 1.20.0)[111]. Prevalence-based filtering with a threshold of 0.5 ensured the removal of features enriched in negative controls. For the 18 S data further steps were applied to refine the datasets. Non-fungal taxa (e.g. Bacteria, Archaea, Apicomplexa, Foraminifera, and host associated ASVs) were deleted using sequence-alignment and taxonomy-based filtering approaches. Filtered ASV tables and representative trees were exported for downstream analyses in R.

Alpha and beta diversity

Alpha diversity metrics were calculated using the `iNEXT` (v. 3.0.1)[112] package in the R environment. Both Hill-Simpson ($q = 2$) and Hill-Shannon ($q = 1$) diversity indices were calculated to quantify sample diversity, based on coverage-rarefied data at 99.5% sample completeness. These metrics account for differences in sequencing depth and ensure robust comparisons between samples. To investigate the effect of copy number correction, raw abundance data were adjusted by estimated 16S gene copy numbers, and a `phyloseq` (v. 1.48.0)[113] object was created with the corrected data. Absolute abundance data were scaled to match the total read count of raw data, followed by rounding to integers to comply with `iNEXT` requirements. Analyses were conducted on three datasets: raw read counts, copy number-corrected counts, and relative abundance data. Alpha diversity trends were displayed as boxplots and scatterplots, with annotations for statistical significance. Beta diversity was assessed using Bray-Curtis dissimilarities, computed based on the lowest sequencing depth (1679 for bacteria, 20 for yeasts) across samples and averaged over 1000 iterations using the "avgdist" function from the `vegan` (v. 2.6-6.1) package. The general number of reads for the 18S rRNA gene sequencing was low (mean reads 280), but the Good's coverage for the samples were acceptable (>99%), so we kept also low read samples (>20 reads) for downstream analysis. These dissimilarities were used to generate principal coordinate analyses (PCoA). PCoA results were overlaid with significant taxonomic vectors fitted using the "envfit" function. Taxonomic vectors for 16 S and 18 S data were fitted separately at the ASV level. To ensure plot clarity, cutoff values for the correlation coefficient (r) were adjusted, with 16 S data filtered at $r > 0.3$ and 18 S data at $r > 0.1$, reducing the number of displayed vectors for enhanced interpretability. Taxa with significant contributions ($p < 0.05$) were visualized on PCoA plots, with vector lengths scaled for clarity. The integration of 18S data into the 16S PCoA allowed for cross-domain ecological insights. PCoA plots incorporated color-coded sample groupings and labeled significant vectors for enhanced interpretability.

18S qPCR

For the 18 S qPCR assay, the selected target is an ASV from the genus *Kurtzmaniella*, chosen based on its high abundance across all samples and high prevalence within the dataset. This sequence was used as the PCR template for Primer-BLAST[114], with a target PCR product size between 70 and 200 bp and a primer melting temperature of 60 °C. The search was enabled to be specific to the PCR template with defined unintended taxa *Homo sapiens*, *Bos taurus*, Apicomplexa, Bacteria and Fungi and had at least three total mismatches to these targets. A list of ten suggested primer pairs were consequently checked for PCR products on potentially unintended templates, product length, melting temperature, self (3') complementarity. The worst delta *G* values for hairpin, and hetero-dimer formations were determined using IDT OligoAnalyzer™ Tool[115]. Additionally, the target was split into 20 kmers and matched to all ASVs from the amplicon sequencing, to identify regions of the target with the least overlap with off target ASVs (Supplementary Fig. 35). The finally selected forward primer pair "PP9" (fwd: 5'- TTC TGG CTA ACC ATT CGC CC -3'/ rev: 5'- ACT GAA TAC TGA TGC CCC CG -3') had a Tm of 60.39 °C and 59.53 °C, a self complementarity of 6 and 2, a self 3' complementarity of 3 and 2, a hairpin worst delta G of -1.36 and 1.43 and a self-dimer worst delta G of -6.21 and -3.61, respectively. The hetero-dimer worst delta G was -6.21. The primer pair matches three additional ASVs, which were consequently considered when calculating the absolute abundances. Before running the qPCR the primers were tested on target and off-target isolates, and showed no non-specific

reactions. The qPCR was optimized using a gradient PCR (46°−60 °C for annealing) and different primer concentrations (i.e. 200 nM, 250 nM, 400 nM). Additionally, to evaluate the homogeneity of the PCR products, dissociation curves were carried out at the end of the qPCR experiments by following a three-step procedure (95 °C, 60 °C, 95 °C). The optimized qPCR was performed on the qTOWER^3 thermocycler (Analytik Jena AG, Jena, Germany), and data processing was carried out with the software qPCRsoft 4.1 (Analytik Jena AG). The DNA samples were run in duplicate. The final reaction contained 0.06 U/μl PlatinumTM Taq DNA Polymerase (Invitrogen™), 1 × TaqMan PCR buffer, 3 mM $MgCl_2$, 200 nM of each primer, 1 × EvaGreen® Dye (Jena Bioscience, Jena, Germany), and 200 nM dNTP Mix (Thermo Scientific™). The final copy numbers of the 18S rRNA gene, as determined by qPCR, were calculated considering the amount of meat used for the cell pellet, pre-extraction dilutions, and DNA extraction volumes. DNA standard curves were generated by plotting the quantification cycle (Cq) values against the log of the initial DNA concentration of purified genomic DNA from isolate ID-0367. The results were used to calculate the absolute abundances of the 18S data.

Individual estimated growth curves

Absolute abundances of bacterial 16S data were calculated using spiked-in controls (details about the spike-in controls see chapter Cell pellet preparation, DNA extraction and amplicon sequencing and processing). Relative abundances were first computed using the `phyloseq` package. The relative abundances of the spiked-in controls were then used to estimate absolute 16S rRNA gene copies per sample. For each sample, the absolute gene copies (A_i) of all detected taxa (i) were estimated using the spiked-in controls' known gene copies (C_{spike}). The calculation was performed using the following formula:

$$A_i = \frac{C_{spike}}{\text{Rel}_{\text{spike}}} \cdot \text{Rel}_i \quad (1)$$

where C_{spike} represents the known absolute copy number of the spike-in, $\text{Rel}_{\text{spike}}$ is the relative abundance of the spike-in in the sequencing data, and Rel_i is the relative abundance of taxon *i*.

Further corrections for 16S rRNA gene copy numbers were performed using the rrnDB database (v. 5.8)[116]. If species-level copy number data were unavailable, the mean copy number (CN_i) from the next higher taxonomic rank was used. Corrected abundances (A_i') were calculated as:

$$A_i' = \frac{A_i}{CN_i} \quad (2)$$

Corrected abundance data were generated at ASV, species, and genus levels and visualized using taxa plots and heatmaps. Growth curves and heatmaps of normalized abundance trends over time were created with `ggplot2`[117] to illustrate the dynamics of highly abundant taxa. For downstream analyses, the *Imtechella*-based absolute abundance dataset was used.

Absolute abundances of fungal taxa were determined using qPCR-derived total genomic equivalents. Matching ASVs for the primer pair used in qPCR were identified, and the sum of their relative abundances ($\text{Rel}_{\text{match}}$) was calculated for each sample. These sums were scaled by the total genomic equivalents (C_{qPCR}) from qPCR results to derive absolute abundances (A_{fungi}) of fungal ASVs:

$$A_{\text{fungi}} = \frac{C_{\text{qPCR}}}{\text{Rel}_{\text{match}}} \quad (3)$$

The absolute abundances of the individual fungal ASVs were calculated using the same formula as for bacterial taxa. Phyloseq objects containing relative and absolute abundances were generated at both ASV and genus levels.

Detection limits for bacterial taxa were calculated for each sample based on sequencing depth (N) and potential prevalence ($P = 0.95$). The detection limit (DL) was defined as:

$$\text{DL} = \log_{10}\left(\left(1-(1-P)^{\frac{1}{N}}\right) \cdot \text{MeanCounts}\right) \quad (4)$$

where MeanCounts represents the mean copy number corrected abundance per sample. These detection limits were included as error bars in taxonomic growth curve plots.

Data visualization included taxonomic growth curves, error bars indicating detection limits, and heatmaps of normalized abundances over time. All plots were generated using `ggplot2` and related R packages. Taxa were filtered to include only those with sufficient contributions for clarity in visual representation. Growth curves were smoothed using the loess method, with standard errors displayed as shaded areas. Heatmaps were generated using `ggplot2`, with taxa ordered by normalized abundance trends over time. The color gradient represented the normalized abundance of each taxon, with maximum values set to 1 for each ASV or genus.

Comparison of culture-dependent and -independent quantification methods

To evaluate the consistency between culture-dependent and -independent quantification methods, we assessed the relationship between colony-forming units (CFU) on culture media and genomic equivalents (GE) derived from amplicon sequencing (16S rRNA) or gene copies derived from qPCR-based (18S rRNA) methods. Normality of the data was assessed visually using Q-Q plots. The data for the comparison of CFU with qPCR were normally distributed. Given the nature of the sampling, with all samples older than 15 days showing similar bacterial loads, the bacterial CFU and GE data were not normally distributed. Despite this, Pearson's correlation was used based on the following criteria: i) the large sample size ($n = 90$), allowing for the Central Limit Theorem to apply to the sampling distribution of the correlation coefficient; ii) the linear relationship between CFU and GE, and iii) the homoscedasticity of the data, both observed in scatterplots (Supplementary Fig. 3a, b).

CoNet analysis

To investigate microbial associations between bacterial and fungal taxa, we constructed an association network using the CoNet (v. 1.1.1.beta)[24] plugin in Cytoscape (v. 3.10.0)[118]. CoNet analysis was performed using relative abundance data, consistent with its default implementation and statistical framework. While absolute abundances were available, their use in cross-domain networks (e.g., bacteria-fungi) was limited due to differences in scale and quantification approach. The network served as a heuristic guide for co-cultivation experiments, and results should be interpreted as hypothesis-generating rather than confirmatory. The network was built using z-scaled, log-transformed relative abundances of 16S rRNA and 18S rRNA amplicon sequencing data. We employed a multi-method approach combining both correlation- and similarity-based association metrics: i) spearman correlation (threshold: ± 0.3), ii) mutual information (threshold: 0.05, 'mi.shrink' method was selected for the MI calculation, with equal frequency binning applied and the JS divergence method for estimating the MI), and iii) Bray-Curtis dissimilarity (threshold: 0.5). In the "Merge menu", the multigraph option was selected, using a mean score merge, a union network merge and a minimum number of two methods that should support a link connecting two nodes. Alpha correction for multiple hypothesis testing was performed using False Discovery Rate (FDR) with a cutoff of 0.05. The randomization included 1,000 iterations using a "edgeScores" routine, a "shuffle_both" resampling strategy, Brown's method[119] for *p*-value merging and a renormalization of the randomization results. For visualization, edges were filtered using a weight threshold of >0.414, and the "Prefuse Force-Directed Layout" was applied, using mutual information-based weights for edge arrangement.

Co-cultivation experiments

Seven LAB, three Enterobacterales, and four yeast strains isolated from vacuum-packed meat were used for the co-culturing experiment to

investigate microbial interactions. All strains were initially cultured in YPD medium at 25 °C under shaking (125 × rpm) for 48 h. Stocks were prepared by mixing 1:2 (v/v) with fresh medium containing 50% glycerol, resulting in a final glycerol concentration of 25%. Stocks were aliquoted and stored at −20 °C. For experiments, aliquots were thawed, and a 1:10 dilution series in PBS was plated for colony-forming unit (CFU) enumeration. Strain-specific media and conditions were used: MRS (LAB, 25 °C anaerobic, 48 h), VRBG (*Serratia liquefaciens*, *Kluyvera intermedia*, 37 °C, 24 h), TSA-Y (*Serratia proteamaculans*, 25 °C, 48 h), and YGC (yeasts, 25 °C, 48 h).

Semi-logarithmic dilutions of stocks were prepared to generate growth curves. A sterile 96-well microplate (Cellstar® U-bottom, clear with lid, GreinerBio-One GmbH, Frickenhausen, Germany) was filled with 100 μl of each dilution, incubated at 25 °C, and optical density (OD) at 595 nm was recorded every 5 min using a microplate reader (Infinite® F200, Tecan, Männedorf, Switzerland). Growth lag phases were manually calculated based on the onset of growth and time intervals between semi-logarithmic steps. These calculations informed the synchronization of microbial growth curves, with bacterial strains occasionally delayed (6–7 h) to align growth phases with yeast partners. Growth curves were accepted as synchronized if they had overlapping exponential growth phases.

For co-culture experiments, each pair of strains was tested in duplicate across two independent experiments. Bacterial and fungal dilutions were prepared at twice the final concentration in YPD + 0.1% L-cysteine. In 96-well plates, 50 μl of fungal solution was combined with 50 μl of bacterial solution (immediately or after 7 h for delayed bacterial inoculation). Monocultures were prepared as controls by replacing the bacterial or fungal solution with fresh medium. Broth only preparations were used as a negative control. Plates were sealed with parafilm to reduce oxygen availability, creating an environment more similar to the low-oxygen conditions of vacuum-packed meat and the growth preferences of LAB.

After ~48 h of incubation at 25 °C, one of the duplicates was used for CFU enumeration. For bacterial CFU determination, media (MRS, VRBG, TSA-Y) were supplemented with 50 μg ml^{-1} cycloheximide (Sigma-Aldrich) and 0.05 μg ml^{-1} micafungin (Sigma-Aldrich)[120] to inhibit fungal growth, while yeast CFU counts used YGC. The second duplicate was used for DNA extraction (Nucleospin microbial kit, Machery-Nagel, Düren, Germany), followed by 16 S and 18 S qPCR for mono- and co-cultures using the BactQuant[121] and FungiQuant systems[122].

Growth curves were analyzed to assess for increased initial growth rates in co-culture compared to monoculture controls. CFU and qPCR results were analyzed for relative increases in carrying capacity, calculated as the ratio of CFU counts or genomic equivalents in co-culture versus monoculture. Increased initial growth rates and carrying capacity were evaluated separately.

Supernatant experiments

For each isolate 10^4 cells were inoculated into 5 ml YPD medium + 0.1% L-cysteine and incubated at 25 °C for 48 h under shaking. The cultures were spun down for 10 min at 8000 × rcf. The supernatants were filtered using a 0.2 μm filter (Filtropur S, Sarstedt AG & Co. KG, Nümbrecht, Germany) and stored at −20 °C until further processing. This cell-free supernatants were used for the following experiments. Target cells were diluted to a concentration of 10^4 cells/ml in YPD medium + 0.1% L-cysteine. 50 μl of the target cells were then mixed with either 50 μl of the cell-free supernatant, 50 μl of fresh YPD medium + 0.1% L-cysteine or 50 μl of a 1:2 (v/v) mix of the cell-free supernatant and fresh YPD medium + 0.1% L-cysteine. The mixtures were incubated at 25 °C in a microplate reader (either Spark® or Infinite® F200, both Tecan) for either 48 h (*Enterobacteriaceae*) or 72 h (for LAB and yeast), with OD595 measurements taken every 5 min after 30 s of shaking. At the end of the incubation the pH of the cultures was measured using a InLab® Micro electrode with a FiveEasy pH meter (Mettler Toledo, Greifensee, Switzerland). The growth curves were analyzed for increased carrying capacity and prolonged lag-phases in the presence of the cell-free supernatants compared to the controls.

Data availability

All sequencing data supporting the findings of this study are openly available in the following repositories: 16S and 18S rRNA gene amplicon sequencing data and MinION whole genome sequencing data of microbial isolates from food samples have been deposited in the European Nucleotide Archive (ENA) under the study accession numbers PRJEB89490 (amplicon sequencing) and PRJEB89493 (WGS). The Sanger sequencing data, presented in FASTA format, are available on GitHub at https://github.com/ffroch/BeiRip.All used codes are available on GitHub at https://github.com/ffroch/BeiRip. This repository contains all relevant scripts used for the analysis.

Received: 1 April 2025; Accepted: 7 June 2025;
Published online: 18 June 2025

References

1. OECD. *Meat Consumption (indicator)*. https://data.oecd.org/agroutput/meat-consumption.htm (2023).
2. Poore, J. & Nemecek, T. Reducing food's environmental impacts through producers and consumers. *Science* **360**, 987–992 (2018).
3. United Nations Department of Economic and Social Affairs; United Nations. *The Sustainable Development Goals Report 2022*. https://unstats.un.org/sdgs/report/2022/ (2022).
4. Yost, C. K. & Nattress, F. M. Molecular typing techniques to characterize the development of a lactic acid bacteria community on vacuum-packaged beef. *Int. J. Food Microbiol.* **72**, 97–105 (2002).
5. Pellissery, A. J., Vinayamohan, P. G., Amalaradjou, M. A. R. and Venkitanarayanan, K. Spoilage bacteria and meat quality. In *Meat Quality Analysis* 307–334 (Elsevier, 2020).
6. Djordjevic, J. et al. Vacuum and modified atmosphere packaging effect on enterobacteriaceae behaviour in minced meat. *J. Food Process. Pres.* **41**, e12837 (2017).
7. Pothakos, V., Devlieghere, F., Villani, F., Björkroth, J. & Ercolini, D. Lactic acid bacteria and their controversial role in fresh meat spoilage. *Meat Sci.* **109**, 66–74 (2015).
8. Erichsen, I. & Molin, G. Microbial flora of normal and high pH beef stored at 4 c in different gas environments. *J. Food Protect.* **44**, 866–869 (1981).
9. Dainty, R. H. & Mackey, B. M. The relationship between the phenotypic properties of bacteria from chill-stored meat and spoilage processes. *Soc. Appl. Bacteriol. Symposium Series* **21**, 103S–14S (1992).
10. Doulgeraki, A. I., Ercolini, D., Villani, F. & Nychas, G.-J. E. Spoilage microbiota associated to the storage of raw meat in different conditions. *Int. J. Food Microbiol.* **157**, 130–141 (2012).
11. de Filippis, F., La Storia, A., Villani, F. & Ercolini, D. Exploring the sources of bacterial spoilers in beefsteaks by culture-independent high-throughput sequencing. *PLoS ONE* **8**, e70222 (2013).
12. Dorn-In, S., Führer, L., Gareis, M. & Schwaiger, K. Cold-tolerant microorganisms causing spoilage of vacuum-packed beef under time-temperature abuse determined by culture and qPCR. *Food Microbiol.* **109**, 104147 (2023).
13. Casaburi, A., Piombino, P., Nychas, G.-J., Villani, F. & Ercolini, D. Bacterial populations and the volatilome associated to meat spoilage. *Food Microbiol.* **45**, 83–102 (2015).
14. Christopher, F. M., Seideman, S. C., Carpenter, Z. L., Smith, G. C. & Vanderzant, C. Microbiology of beef packaged in various gas atmospheres. *J. Food Protect.* **42**, 240–244 (1979).
15. Pennacchia, C., Ercolini, D., Villani, F. Spoilage-related microbiota associated with chilled beef stored in air or vacuum pack. *Food Microbiol*. **28**, 84–93 (2011).
16. Fontana, C., Cocconcelli, P. S. & Vignolo, G. Direct molecular approach to monitoring bacterial colonization on vacuum-packaged beef. *Appl. Environ. Microb.* **72**, 5618–5622 (2006).

17. Jääskeläinen, E., Hultman, J., Parshintsev, J., Riekkola, M.-L. & Björkroth, J. Development of spoilage bacterial community and volatile compounds in chilled beef under vacuum or high oxygen atmospheres. *Int. J. Food Microbiol.* **223**, 25–32 (2016).
18. de Freitas, C. F. et al. Bacterial microbiota shifts in vacuum-packed beef during storage at different temperatures: Impacts on blown pack spoilage. *Food Microbiol.* **119**, 104448 (2024).
19. Hultman, J., Johansson, P. & Björkroth, J. Longitudinal metatranscriptomic analysis of a meat spoilage microbiome detects abundant continued fermentation and environmental stress responses during shelf life and beyond. *Appl. Environ. Microb.* **86**, e01575–20 (2020).
20. Tofalo, R. et al. The life and times of yeasts in traditional food fermentations. *Crit. Rev. Food Sci.* **60**, 3103–3132 (2020).
21. Kabisch, J. et al. Spoilage of vacuum-packed beef by the yeast kazachstania psychrophila. *Food Microbiol.* **53**, 15–23 (2016).
22. Irlinger, F. & Mounier, J. Microbial interactions in cheese: Implications for cheese quality and safety. *Curr. Opin. Biotech.* **20**, 142–148 (2009).
23. Cosetta, C. M., Kfoury, N., Robbat, A. & Wolfe, B. E. Fungal volatiles mediate cheese rind microbiome assembly. *Environ. Microbiol.* **22**, 4745–4760 (2020).
24. Faust, K. & Raes, J. CoNet app: Inference of biological association networks using cytoscape. *F1000Research* **5**, 1519 (2016).
25. Leclercq-Perlat, M. N., Oumer, A., Bergere, J. L., Spinnler, H. E. & Corrieu, G. Behavior of brevibacterium linens and debaryomyces hansenii as ripening flora in controlled production of smear soft cheese from reconstituted milk: Growth and substrate consumption dairy foods. *J. Dairy Sci.* **83**, 1665–1673 (2000).
26. Beyer, L. et al. Coordination of FocA and pyruvate formate-lyase synthesis in escherichia coli demonstrates preferential translocation of formate over other mixed-acid fermentation products. *J. Bacteriol.* **195**, 1428–1435 (2013).
27. Casiano-Colón, A. & Marquis, R. E. Role of the arginine deiminase system in protecting oral bacteria and an enzymatic basis for acid tolerance. *Appl. Environ. Microb.* **54**, 1318–1324 (1988).
28. Kolbeck, S., Abele, M., Hilgarth, M. & Vogel, R. F. Comparative proteomics reveals the anaerobic lifestyle of meat-spoiling pseudomonas species. *Front. Microbiol.* **12**, 664061 (2021).
29. Ercolini, D. et al. Monitoring of microbial metabolites and bacterial diversity in beef stored under different packaging conditions. *Appl. Environ. Microb.* **77**, 7372–7381 (2011).
30. Johansson, P. et al. ICoMST 2020 review papers. *Meat Muscle Biol.* **4**, 12 (2020).
31. Shao, L. et al. Advances in understanding the predominance, phenotypes, and mechanisms of bacteria related to meat spoilage. *Trends Food Sci.Technol.* **118**, 822–832 (2021).
32. Ponomarova, O. et al. Yeast creates a niche for symbiotic lactic acid bacteria through nitrogen overflow. *Cell Syst.* **5**, 345–357.e6 (2017).
33. Gabrielli, N. et al. Unravelling metabolic cross-feeding in a yeast-bacteria community using 13 c-based proteomics. *Mol. Sys. Biol.* **19**, e11501 (2023).
34. Santos, N. N. et al. Hydrolysis of pork muscle sarcoplasmic proteins by debaryomyces hansenii. *Int. J. Microbiolo.* **68**, 199–206 (2001).
35. Durá, M. A., Flores, M. & Toldrá, F. Effect of debaryomyces spp. On the proteolysis of dry-fermented sausages. *Meat Sci.* **68**, 319–328 (2004).
36. Zinjarde, S. S. Food-related applications of yarrowia lipolytica. *Food Chem.* **152**, 1–10 (2014).
37. Čanak, I. et al. Purification and characterization of a novel cold-active lipase from the yeast candida zeylanoides. *J. Mol. Microb. Biotech.* **25**, 403–411 (2015).
38. Ismail, S. A. Presence and changes in populations of yeasts on raw and processed poultry products stored at refrigeration temperature. *Int. J. Food Microbiol.* **62**, 113–121 (2000).
39. Yalcin, H. T. & Ucar, F. B. Isolation and characterization of cheese spoiler yeast isolated from turkish white cheeses. *Ann. Microbiol.* **59**, 477–483 (2009).
40. Belák, Á. et al. Molecular analysis of poultry meat spoiling microbiota and heterogeneity of their proteolytic and lipolytic enzyme activities. *Acta Alimentaria* **40**, 3–22 (2011).
41. Hube, B. & Naglik, J. Candida albicans proteinases: Resolving the mystery of a gene family. *Microbiology* **147**, 1997–2005 (2001).
42. Fröhlich-Wyder, M.-T., Arias-Roth, E. & Jakob, E. Cheese yeasts. *Yeast* **36**, 129–141 (2019).
43. Riesute, R., Salomskiene, J., Moreno, D. S. & Gustiene, S. Effect of yeasts on food quality and safety and possibilities of their inhibition. *Trends Food Sci. Tech.* **108**, 1–10 (2021).
44. Ibrahim, S. A.et al. Lactic acid bacteria as antimicrobial agents: Food safety and microbial food spoilage prevention. *Foods (Basel, Switzerland)* **10**, 3131 (2021).
45. Barcenilla, C., Ducic, M., López, M., Prieto, M. & Álvarez-Ordóñez, A. Application of lactic acid bacteria for the biopreservation of meat products: A systematic review. *Meat Sci.* **183**, 108661 (2022).
46. Rimaux, T. et al. Expression of the arginine deiminase pathway genes in lactobacillus sakei is strain dependent and is affected by the environmental pH. *Appl. Environ. Microbiol.* **78**, 4874–4883 (2012).
47. Xu, S. et al. MicrobiotaProcess: A comprehensive r package for deep mining microbiome. *Innovation* **4**, 100388 (2023).
48. Zhang, P., Baranyi, J. & Tamplin, M. Interstrain interactions between bacteria isolated from vacuum-packaged refrigerated beef. *Appl. Environ. Microb.* **81**, 2753–2761 (2015).
49. Choudhary, B., Nagpure, A. & Gupta, R. K. Fungal cell-wall lytic enzymes, antifungal metabolite(s) production, and characterization from streptomyces exfoliatus MT9 for controlling fruit-rotting fungi. *J. Basic Microbiol.* **54**, 1295–1309 (2014).
50. Palumbo, J. D., Yuen, G. Y., Jochum, C. C., Tatum, K. & Kobayashi, D. Y. Mutagenesis of beta-1,3-glucanase genes in lysobacter enzymogenes strain C3 results in reduced biological control activity toward bipolaris leaf spot of tall fescue and pythium damping-off of sugar beet. *Phytopathology* **95**, 701–707 (2005).
51. Bundock, P., Dulk-Ras, Aden,Beijersbergen,A. & Hooykaas, P. J. Trans-kingdom t-DNA transfer from agrobacterium tumefaciens to saccharomyces cerevisiae. *EMBO J.* **14**, 3206–3214 (1995).
52. Smeets, L. C. & Kusters, J. G. Natural transformation in helicobacter pylori: DNA transport in an unexpected way. *Trends Microbiol.* **10**, 159–162 (2002).
53. Trunk, K. et al. The type VI secretion system deploys antifungal effectors against microbial competitors. *Nat. Microbiol.* **3**, 920–931 (2018).
54. Leveau, J. H. J. & Preston, G. M. Bacterial mycophagy: definition and diagnosis of a unique bacterial-fungal interaction. *New Phytol.* **177**, 859–876 (2008).
55. Hunziker, L. et al. Pseudomonas strains naturally associated with potato plants produce volatiles with high potential for inhibition of phytophthora infestans. *Appl. Environ. Microb.* **81**, 821–830 (2015).
56. Matilla, M. A., Leeper, F. J. & Salmond, G. P. C. Biosynthesis of the antifungal haterumalide, oocydin a, in serratia, and its regulation by quorum sensing, RpoS and hfq. *Environ. Microbiol.* **17**, 2993–3008 (2015).
57. de Vrieze, M. et al. Volatile organic compounds from native potato-associated pseudomonas as potential anti-oomycete agents. *Front. Microbiol.* **6**, 1295 (2015).
58. Netzker, T., Shepherdson, E. M. F., Zambri, M. P. & Elliot, M. A. Bacterial volatile compounds: Functions in communication, cooperation, and competition. *Annu. Rev. Microbiol.* **74**, 409–430 (2020).
59. Carter-House, D., Chung, J., McDonald, S., Mauck, K. and Stajich, J. E. Volatiles from serratia marcescens, s. Proteamaculans, and

bacillus subtilis inhibit growth of rhizopus stolonifer and other fungi. *bioRxiv* https://doi.org/10.1101/2020.09.07.286443 (2020).
60. Walsh, P. S., Metzger, D. A. & Higuchi, R. Chelex 100 as a medium for simple extraction of DNA for PCR-based typing from forensic material. BioTechniques 10(4): 506-13 (april 1991). *BioTech.* **54**, 134–139 (2013).
61. Edgcomb, V. et al. Protistan microbial observatory in the cariaco basin, caribbean. I. Pyrosequencing vs sanger insights into species richness. *ISME J.* **5**, 1344–1356 (2011).
62. R Core Team. *R: A Language and Environment for Statistical Computing*. https://www.r-project.org/ (2024).
63. Chao, K.-H., Barton, K., Palmer, S. & Lanfear, R. sangeranalyseR: Simple and interactive processing of sanger sequencing data in r. *Genome Biol. Evol.* **13**, evab028 (2021).
64. Callahan, B. J. et al. DADA2: High-resolution sample inference from illumina amplicon data. *Nat. Methods* **13**, 581–583 (2016).
65. Callahan, B. Silva taxonomic training data formatted for DADA2 (silva version 138.2). *Zenodo* https://doi.org/10.5281/zenodo.14169025 (2024).
66. Ali, A., DADA2 formatted 16S rRNA gene sequences for both bacteria & archaea. *Zenodo* https://doi.org/10.5281/zenodo.2541238 (2024).
67. McLaren, M. R., Silva SSU taxonomic training data formatted for DADA2 (silva version 138). *Zenodo* https://doi.org/10.5281/zenodo.3731174 (2020).
68. Wright, E. S. Using DECIPHER v2.0 to analyze big biological sequence data in r. *R J.* **8**, 352–359 (2016).
69. Bodenhofer, U., Bonatesta, E., Horejš-Kainrath, C. & Hochreiter, S. Msa: An r package for multiple sequence alignment. *Bioinformatics* **31**, 3997–3999 (2015).
70. Edgar, R. C. MUSCLE: Multiple sequence alignment with high accuracy and high throughput. *Nucleic Acids Res.* **32**, 1792–1797 (2004).
71. Castresana, J. Selection of conserved blocks from multiple alignments for their use in phylogenetic analysis. *Mol. Biol. Evol.* **17**, 540–552 (2000).
72. Yu, G., Smith, D. K., Zhu, H., Guan, Y. & Lam, T. T.-Y. Ggtree : An r package for visualization and annotation of phylogenetic trees with their covariates and other associated data. *Methods Ecol. Evol.* **8**, 28–36 (2017).
73. Hackathon, R. et al. *Phylobase: Base Package For Phylogenetic Structures And Comparative Data*. https://github.com/fmichonneau/phylobase (2024).
74. Oxford Nanopore Technologies. *Dorado*. https://github.com/nanoporetech/dorado (2024).
75. Oxford Nanopore Technologies. *Nanopore-only Microbial Isolate Sequencing Solution (No-miss) - Rapid Barcoding Kit V14 (SQK-RBK114.24 or SQK-RBK114.96)*. https://nanoporetech.com/document/no-miss-isolate-sequencing-rapid-barcoding-v14?format=versions (2024).
76. Oxford Nanopore Technologies. *Bacteria gDNA Extraction For Nanopore-only Microbial Isolate Sequencing Solution (NO-MISS)*. https://nanoporetech.com/document/extraction-method/bact-gdna-no-miss (2024).
77. Oxford Nanopore Technologies. *Fungi gDNA Extraction For Nanopore-only Microbial Isolate Sequencing Solution (NO-MISS)*. https://nanoporetech.com/document/extraction-method/fungi-gdna-no-miss (2024).
78. Wick, R. *Filtlong*. https://github.com/rrwick/filtlong (2021).
79. Kolmogorov, M., Yuan, J., Lin, Y. & Pevzner, P. A. Assembly of long, error-prone reads using repeat graphs. *Nat. Biotechnol.* **37**, 540–546 (2019).
80. Oxford Nanopore Technologies. *Medaka*. https://github.com/nanoporetech/medaka (2022).
81. Parks, D., Skennerton, C. & Imelfor, M. *CheckM*. https://github.com/ecogenomics/CheckM (2024).
82. Chaumeil, P.-A., Mussig, A. J., Hugenholtz, P. & Parks, D. H. GTDB-tk v2: Memory friendly classification with the genome taxonomy database. *Bioinformatics* **38**, 5315–5316 (2022).
83. Parks, D. H. et al. GTDB: An ongoing census of bacterial and archaeal diversity through a phylogenetically consistent, rank normalized and complete genome-based taxonomy. *Nucleic Acids Res.* **50**, D785–D794 (2022).
84. Seemann, T. Prokka: Rapid prokaryotic genome annotation. *Bioinformatics* **30**, 2068–2069 (2014).
85. Vaser, R., Sović, I., Nagarajan, N. & Šikić, M. Fast and accurate de novo genome assembly from long uncorrected reads. *Genome Res.* **27**, 737–746 (2017).
86. Wood, D. E., Lu, J. & Langmead, B. Improved metagenomic analysis with kraken 2. *Genome Biol.* **20**, 257 (2019).
87. Altschul, S. F., Gish, W., Miller, W., Myers, E. W. & Lipman, D. J. Basic local alignment search tool. *J. Mol. Biol.* **215**, 403–410 (1990).
88. Manni, M., Berkeley, M. R., Seppey, M., Simão, F. A. & Zdobnov, E. M. BUSCO update: Novel and streamlined workflows along with broader and deeper phylogenetic coverage for scoring of eukaryotic, prokaryotic, and viral genomes. *Mol. Biol. Evol.* **38**, 4647–4654 (2021).
89. Jain, C., Rodriguez-R, L. M., Phillippy, A. M., Konstantinidis, K. T. & Aluru, S. High throughput ANI analysis of 90K prokaryotic genomes reveals clear species boundaries. *Nat. Commun.* **9**, 5114 (2018).
90. Haese-Hill, W., Crouch, K. & Otto, T. D. Annotation and visualization of parasite, fungi and arthropod genomes with companion. *Nucleic Acids Res.* **52**, W39–W44 (2024).
91. Blin, K. et al. antiSMASH 7.0: New and improved predictions for detection, regulation, chemical structures and visualisation. *Nucleic Acids Res.* **51**, W46–W50 (2023).
92. Huerta-Cepas, J. et al. eggNOG 5.0: A hierarchical, functionally and phylogenetically annotated orthology resource based on 5090 organisms and 2502 viruses. *Nucleic Acids Res.* **47**, D309–D314 (2019).
93. Cantalapiedra, C. P., Hernández-Plaza, A., Letunic, I., Bork, P. & Huerta-Cepas, J. eggNOG-mapper v2: Functional annotation, orthology assignments, and domain prediction at the metagenomic scale. *Mol. Biol. Evol.* **38**, 5825–5829 (2021).
94. Kanehisa, M. et al. KEGG for linking genomes to life and the environment. *Nucleic Acids Res.* **36**, D480–4 (2008).
95. Zheng, J. et al. dbCAN3: Automated carbohydrate-active enzyme and substrate annotation. *Nucleic Acids Res.* **51**, W115–W121 (2023).
96. Machado, D., Andrejev, S., Tramontano, M. & Patil, K. R. Fast automated reconstruction of genome-scale metabolic models for microbial species and communities. *Nucleic Acids Res.* **46**, 7542–7553 (2018).
97. Stämmler, F. et al. Adjusting microbiome profiles for differences in microbial load by spike-in bacteria. *Microbiome* **4**, 28 (2016).
98. Kallastu, A. et al. Absolute quantification of viable bacteria abundances in food by next-generation sequencing: Quantitative NGS of viable microbes. *Curr. Res. Food Sci.* **6**, 100443 (2023).
99. Oshiro, M., Nakamura, K. & Tashiro, Y. *Biosci. Biotechnol. Biochem.* **89**, 294–303 (2025).
100. Qiagen. *DNeasy PowerFood Microbial Kit Handbook*. https://www.qiagen.com/at/resources/resourcedetail?id=55456cd5-2de4-43b2-8eaa-760d1371710a&lang=en (2017).
101. Klindworth, A. et al. Evaluation of general 16S ribosomal RNA gene PCR primers for classical and next-generation sequencing-based diversity studies. *Nucleic Acids Res.* **41**, e1 (2013).
102. Hugerth, L. W. et al. Systematic design of 18S rRNA gene primers for determining eukaryotic diversity in microbial consortia. *PLoS ONE* **9**, e95567 (2014).

103. Vainio, E. J. & Hantula, J. Direct analysis of wood-inhabiting fungi using denaturing gradient gel electrophoresis of amplified ribosomal DNA. *Mycol. Res.* **104**, 927–936 (2000).
104. Guillou, L. et al. The protist ribosomal reference database (PR2): a catalog of unicellular eukaryote small sub-unit rRNA sequences with curated taxonomy. *Nucleic Acids Res.* **41**, D597–604 (2013).
105. Andrews, S. *FastQC*. https://github.com/s-andrews/FastQC (2020).
106. Bolger, A. M., Lohse, M. & Usadel, B. Trimmomatic: A flexible trimmer for illumina sequence data. *Bioinformatics* **30**, 2114–2120 (2014).
107. Ewels, P., Magnusson, M., Lundin, S. & Käller, M. MultiQC: Summarize analysis results for multiple tools and samples in a single report. *Bioinformatics* **32**, 3047–3048 (2016).
108. Bolyen, E. et al. Reproducible, interactive, scalable and extensible microbiome data science using QIIME 2. *Nat. Biotechnol.* **37**, 852–857 (2019).
109. Bokulich, N. A. et al. Optimizing taxonomic classification of marker-gene amplicon sequences with QIIME 2's q2-feature-classifier plugin. *Microbiome* **6**, 90 (2018).
110. Robeson, M. S. et al. RESCRIPt: Reproducible sequence taxonomy reference database management. *PLoS Comput. Biol.* **17**, e1009581 (2021).
111. Davis, N. M., Proctor, D. M., Holmes, S. P., Relman, D. A. & Callahan, B. J. Simple statistical identification and removal of contaminant sequences in marker-gene and metagenomics data. *Microbiome* **6**, 226 (2018).
112. Hsieh, T. C., Ma, K. H. & Chao, A. iNEXT: An r package for rarefaction and extrapolation of species diversity (h ill numbers). *Methods Ecol. Evol.* **7**, 1451–1456 (2016).
113. McMurdie, P. J. & Holmes, S. Phyloseq: An r package for reproducible interactive analysis and graphics of microbiome census data. *PLoS ONE* **8**, e61217 (2013).
114. Ye, J. et al. Primer-BLAST: A tool to design target-specific primers for polymerase chain reaction. *BMC bioinform.* **13**, 134 (2012).
115. Owczarzy, R. et al. IDT SciTools: A suite for analysis and design of nucleic acid oligomers. *Nucleic Acids Res.* **36**, W163–9 (2008).
116. Stoddard, S. F., Smith, B. J., Hein, R., Roller, B. R. K. & Schmidt, T. M. rrnDB: Improved tools for interpreting rRNA gene abundance in bacteria and archaea and a new foundation for future development. *Nucleic Acids Res.* **43**, D593–8 (2015).
117. Wickham, H. *Ggplot2: Elegant Graphics for Data Analysis* 2nd edn, Vol. 260 (Springer, 2016).
118. Shannon, P. et al. Cytoscape: A software environment for integrated models of biomolecular interaction networks. *Genome Res.* **13**, 2498–2504 (2003).
119. Brown, M. B. 400: A method for combining non-independent, one-sided tests of significance. *Biometrics* **31**, 987–992 (1975).
120. Rao, C. et al. Multi-kingdom ecological drivers of microbiota assembly in preterm infants. *Nature* **591**, 633–638 (2021).
121. Liu, C. M. et al. BactQuant: An enhanced broad-coverage bacterial quantitative real-time PCR assay. *BMC Microbiol.* **12**, 56 (2012).
122. Liu, C. M. et al. FungiQuant: A broad-coverage fungal quantitative real-time PCR assay. *BMC Microbiol.* **12**, 255 (2012).

Acknowledgements

This work was supported by the Assistant Professor Tenure Track Program of the University of Veterinary Medicine, Vienna, and the Sparkling Science 2.0 grant (project 'Micro-Tramper') funded by the Austrian Federal Ministry of Science, Research and Economy (BMWFW). N.M.Q. is hired under the Generation D initiative, promoted by Red.es, an organization attached to the Ministry for Digital Transformation and the Civil Service, for the attraction and retention of talent through grants and training contracts, financed by the Recovery, Transformation and Resilience Plan through the European Union's Next Generation funds. M.S.C. is currently funded by The Higher Education Commission (HEC) Scholarship Pakistan.

Author contributions

F.-F.R., C.R.S. and E.S. conceived and planned the experiments. F.-F.R., M.D. and S.M.C. carried out the experiments. F.-F.R., N.M.Q. and T.M. performed the computations. F.-F.R., M.D. and E.S. wrote the manuscript with input from all authors. F.-F.R. and C.R.S. did the final editing. All authors provided critical feedback on the research, analysis, and manuscript.

Competing interests

The authors declare no competing interests.

Additional information

Supplementary information The online version contains supplementary material available at https://doi.org/10.1038/s41538-025-00479-8.

Correspondence and requests for materials should be addressed to Franz-Ferdinand Roch.

Reprints and permissions information is available at http://www.nature.com/reprints

Publisher's note Springer Nature remains neutral with regard to jurisdictional claims in published maps and institutional affiliations.

Open Access This article is licensed under a Creative Commons Attribution-NonCommercial-NoDerivatives 4.0 International License, which permits any non-commercial use, sharing, distribution and reproduction in any medium or format, as long as you give appropriate credit to the original author(s) and the source, provide a link to the Creative Commons licence, and indicate if you modified the licensed material. You do not have permission under this licence to share adapted material derived from this article or parts of it. The images or other third party material in this article are included in the article's Creative Commons licence, unless indicated otherwise in a credit line to the material. If material is not included in the article's Creative Commons licence and your intended use is not permitted by statutory regulation or exceeds the permitted use, you will need to obtain permission directly from the copyright holder. To view a copy of this licence, visit http://creativecommons.org/licenses/by-nc-nd/4.0/.

© The Author(s) 2025